

# Efficient Algorithms for Low Tubal Rank Tensor Approximation with Applications to Image Compression, Super-Resolution and Deep Learning

Salman Ahmadi-Asl<sup>a,b</sup>, Naeim Rezaeian<sup>b</sup>, Cesar F. Caiafa<sup>c</sup>, André L. F. de Almeida<sup>d</sup>

<sup>a</sup>*Lab of Machine Learning and Knowledge Representation, Innopolis University, 420500 Innopolis, Russia, email: s.ahmadiasl@innopolis.ru,*

<sup>b</sup>*Peoples' Friendship University of Russia, Moscow, Russia,*

<sup>c</sup>*Instituto Argentino de Radioastronomía—CCT La Plata, CONICET/CIC-PBA/UNLP, Villa Elisa 1894, Argentina,*

<sup>d</sup>*Department of Teleinformatics Engineering, Federal University of Ceara, Fortaleza, Brazil,*

---

## Abstract

In this paper we propose efficient randomized fixed-precision techniques for low tubal rank approximation of tensors. The proposed methods are faster and more efficient than the existing fixed-precision algorithms for approximating the truncated tensor SVD (T-SVD). Besides, there are a few works on randomized single-pass algorithms for computing low tubal rank approximation of tensors, none of them experimentally reports the robustness of such algorithms for low-rank approximation of real-world data tensors e.g., images and videos. The current single-pass algorithms for tensors are generalizations of those developed for matrices to tensors. However, the single-pass randomized algorithms for matrices have been recently improved and stabilized. Motivated by this progress, in this paper, we also generalize them to the tensor case based on the tubal product (T-product). We conduct extensive simulations to study the robustness of them compared with the existing single-pass randomized algorithms. In particular, we experimentally found that single-pass algorithms with the sketching parameters of equal sizes usually lead to ill-conditioned tensor least-squares problems and inaccurate results. It is experimentally shown that our proposed single-pass algorithms are robust in this sense. Numerical results demonstrate that under the same conditions (setting the same hyper-parameters), our proposed algorithms provide better performance. Three applications to image compression, super-resolution problem and deep learning are also presented.

*Keywords:* Tensors, randomization, single-pass randomized algorithms

*PACS:* 0000, 1111

*2000 MSC:* 0000, 1111

---

## 1. Introduction

Tensor decompositions are useful techniques in a variety of applications such as signal processing, machine learning and deep learning. Tucker decomposition [1, 2], tensor train/ring [3, 4, 5], tensor SVD (T-SVD) [6], Kronecker Tensor decomposition [7, 8, 9], block term decomposition, and constrained factor decompositions [10, 11], are some of the widely used tensor decomposition in the literature. Tensor and tensor decompositions were used in several applications such as tensor completion [12, 13], recommender systems [14], machine learning [15], Hammerstein identification [16], and wireless communications [17, 18, 19, 20, 21].

Computing the mentioned tensor decompositions is prohibitive for large-scale data tensors. Due to this issue, randomized algorithms have been proposed in the past decade to speed up these processes. Indeed, randomized algorithms for tensor decomposition offer several advantages over traditional deterministic methods. They are often faster and more memory-efficient, making them well-suited for large-scale datasets. Additionally, randomized algorithms can provide approximate tensor decompositions with a controlled level of accuracy, allowing for trade-offs between computational cost and degree of approximation. For the randomized algorithms with different types of tensor decompositions, we refer to [22, 23, 24, 25]

With the emergence of big data, more and more large-scale data tensors are generated. Low-rank approximations of such big data tensors are required in several applications, e.g., tensor completion [26], recommender systems [14]. This is a challenging task, especially when they are stored out of core<sup>1</sup> and distributed among several machines because here, the communication cost due to the data movement is the main bottleneck and may exceed the main computation.

Because of this issue, passing the data tensor as few times as possible is crucial. In the context of the randomization framework, such algorithms are called

---

<sup>1</sup>Storing data out-of-core refers to the practice of storing data on disk rather than in memory, particularly when the data size exceeds the available memory capacity of a system. This approach allows for handling large datasets that cannot fit entirely into memory. Several difficulties are associated with storing data out-of-core, such as slower access, increased latency, I/O bottlenecks, data management complexity, etc. We refer [27] to more details.

*pass-efficient* algorithms.

Tensor SVD (T-SVD) is a widely used tensor decomposition, which has been applied in many applications such as image/video completion [28], face recognition [29], compression [30] and so on. It decomposes a tensor as a T-product (to be defined in Section 2) [31] of three tensors similar to the classical SVD for matrices. To deal with large-scale tensors, several randomized algorithms have been proposed to compute a low tubal rank T-SVD [25, 32, 33]. Recently, we proposed a randomized pass-efficient algorithm in [33] for the T-SVD with an application to image/video completion. However, our algorithm was applicable only for  $v \geq 2$  number of passes over the underlying data tensor. It is known that in some applications, we may afford only a one pass and due to this issue, in this paper we would like to propose two efficient single-pass algorithms ( $v = 1$ ). To the best of our knowledge, the only paper, which proposes single-pass randomized algorithms for the T-SVD is [32]. The proposed algorithms in [32] are not optimized in several ways. First of all, the authors do not use the fast T-product and t-QR decomposition introduced in [34]. Second, they are generalizations of those proposed in [35] for matrices to tensors, which have been recently modified and stabilised in [36]. It is worth noting that a single-pass algorithm based on sampling lateral and horizontal slices is also developed in [37], see a graphical illustration on this model in Figure 1. In this model, the intersection tensor of the selected lateral and horizontal slices is considered and its Moore-pseudoinverse of it is set as the middle tensor  $\underline{U}$  in the CUR approximation. This algorithm does not provide satisfying results when the number of frontal and lateral slices are the same due to the same conditioning properties. We report this in the numerical results and compare it with other single-pass randomized algorithms. To overcome this issue, we present several single-pass algorithms for the computation of the T-SVD and extensively compare their performance with the baselines. In particular, we empirically show that our proposed single-pass algorithms are robust in this sense. Moreover, we apply of proposed single-pass randomized algorithms to the image-super resolution and object detection tasks as important computer vision problems. To best of our knowledge, this paper is the first unitizing single-pass algorithms for such computer vision applications.

We also study the randomized fixed-precision algorithms for computing a low tubal rank approximation of third order tensors. Such algorithms are of interest when a given estimation of the tubal rank is not available and for a given approximation error bound, we have to estimate an appropriate tubal rank and the corresponding low tubal rank approximation. We have recently proposed a fixed-precision algorithm in [38]. Inspired by the interesting results reported in [39], we

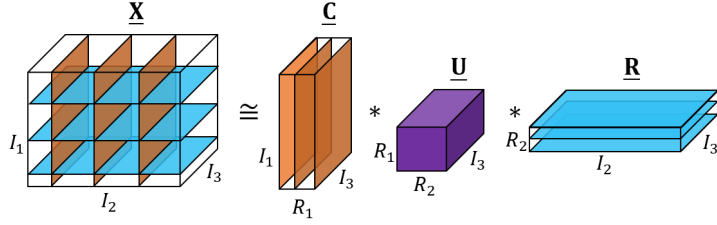


Figure 1: Randomized low tubal rank approximation based on slice sampling [37, 40].

use these techniques to further improve our randomized fixed-precision algorithm to compute a low tubal rank approximation of third order tensors. The extensive simulations provided in this paper, demonstrate that the new proposed randomized fixed-precision algorithm is faster and more efficient.

In summary, our main contributions can be summarized as follows:

- Proposing more efficient and robust randomized fixed-precision algorithms for computing the T-SVD
- Proposing three efficient single-pass algorithms for computation of the T-SVD.
- Providing theoretical guarantees of the proposed algorithms.
- Conducting extensive experimental results on synthetic and real-world data with applications to image/video compression, image super-resolution and deep learning. To the best of our knowledge this is the first paper using single-pass algorithms for tensor completion and image super-resolution.

The paper is structured as follows: In Section 2, we present the preliminary concepts and notations. The T-SVD and existing algorithm for its computation are discussed in Section 3. The proposed single-pass and fixed-precision algorithms are described in Section 4 and 5, respectively with their theoretical results. In Section 6 the experimental results are conducted and finally a conclusion is given in Section 7.

## 2. Background

This section gives a necessary background on tensors and introduces the notation used throughout this paper. Tensors, matrices and vectors are denoted by

underlined bold upper case letters e.g.,  $\underline{\mathbf{X}}$ , bold upper case letters, e.g.,  $\mathbf{X}$  and bold lower case letters, e.g.,  $\mathbf{x}$ , respectively. For a third-order tensor  $\underline{\mathbf{X}}$ , the slices  $\underline{\mathbf{X}}(:, :, k)$ ,  $\underline{\mathbf{X}}(:, j, :)$  and  $\underline{\mathbf{X}}(i, :, :)$  are called frontal, lateral and horizontal slices. We also use the notation  $\underline{\mathbf{X}}_1$  to denote the first frontal slice of the tensor  $\underline{\mathbf{X}}$ . For a third-order tensor  $\underline{\mathbf{X}}$ , the sub-tensor  $\underline{\mathbf{X}}(i, j, :)$  is called a tube. The Frobenius norm of tensors is denoted by  $\|\cdot\|_F$  and the infinity norm of tensors is denoted by  $\|\cdot\|_\infty$ . The notation “conj” denotes the complex conjugate of a complex number or the component-wise complex conjugate of a matrix.  $\lceil n \rceil$  means the nearest integer number greater than or equal to  $n$ . Throughout the paper, we only focus on real-valued tensors, however, our results can be readily generalized to complex-valued tensors.

Two tensors can be concatenated along the first or second modes. A concatenation along mode 1 of tensors  $\underline{\mathbf{A}} \in \mathbb{R}^{I_1 \times I_2 \times I_3}$  and  $\underline{\mathbf{B}} \in \mathbb{R}^{J_1 \times J_2 \times J_3}$  is denoted as  $\underline{\mathbf{C}} = \underline{\mathbf{A}} \boxplus_1 \underline{\mathbf{B}} \in \mathbb{R}^{(I_1+J_1) \times I_2 \times I_3}$ , where  $I_2 = J_2$ ,  $I_3 = J_3$  and the same definition can be stated for concatenation along the second mode. Alternatives notations for the concatenation along the first and second modes are  $\underline{\mathbf{A}} \boxplus_1 \underline{\mathbf{B}} \equiv \begin{bmatrix} \underline{\mathbf{A}} \\ \underline{\mathbf{B}} \end{bmatrix}$  and  $\underline{\mathbf{A}} \boxplus_2 \underline{\mathbf{B}} \equiv [\underline{\mathbf{A}}, \underline{\mathbf{B}}]$ .

**Definition 1.** (T-product) Let  $\underline{\mathbf{X}} \in \mathbb{R}^{I_1 \times I_2 \times I_3}$  and  $\underline{\mathbf{Y}} \in \mathbb{R}^{I_2 \times I_4 \times I_3}$ , then the T-product  $\underline{\mathbf{X}} * \underline{\mathbf{Y}} \in \mathbb{R}^{I_1 \times I_4 \times I_3}$  is defined as follows

$$\underline{\mathbf{C}} = \underline{\mathbf{X}} * \underline{\mathbf{Y}} = \text{fold}(\text{circ}(\underline{\mathbf{X}}) \text{unfold}(\underline{\mathbf{Y}})), \quad (1)$$

where

$$\text{circ}(\underline{\mathbf{X}}) = \begin{bmatrix} \underline{\mathbf{X}}(:, :, 1) & \underline{\mathbf{X}}(:, :, I_3) & \cdots & \underline{\mathbf{X}}(:, :, 2) \\ \underline{\mathbf{X}}(:, :, 2) & \underline{\mathbf{X}}(:, :, 1) & \cdots & \underline{\mathbf{X}}(:, :, 3) \\ \vdots & \vdots & \ddots & \vdots \\ \underline{\mathbf{X}}(:, :, I_3) & \underline{\mathbf{X}}(:, :, I_3 - 1) & \cdots & \underline{\mathbf{X}}(:, :, 1) \end{bmatrix},$$

and

$$\text{unfold}(\underline{\mathbf{Y}}) = \begin{bmatrix} \underline{\mathbf{Y}}(:, :, 1) \\ \underline{\mathbf{Y}}(:, :, 2) \\ \vdots \\ \underline{\mathbf{Y}}(:, :, I_3) \end{bmatrix}, \quad \underline{\mathbf{Y}} = \text{fold}(\text{unfold}(\underline{\mathbf{Y}})).$$

It can be proved that for a tensor  $\underline{\mathbf{X}} \in \mathbb{R}^{I_1 \times I_2 \times I_3}$ , we have

$$\|\underline{\mathbf{X}}\|_F^2 = \frac{1}{I_3} \sum_{i=1}^{I_3} \|\widehat{\underline{\mathbf{X}}}(:, :, i)\|_F^2, \quad (2)$$

where  $\widehat{\underline{\mathbf{X}}}(:, :, i)$  is the  $i$ -th frontal slice of the tensor  $\widehat{\underline{\mathbf{X}}} = \text{fft}(\underline{\mathbf{X}}, [], 3)$ , which calculates the fast Fourier transform of all tubes of the tensor  $\underline{\mathbf{X}}$ , see [34, 25]. Algorithm 2 summarizes the process of T-product of two tensors.

---

**Algorithm 1:** T-product in the Fourier domain [31]

---

**Input :** Two data tensors  $\underline{\mathbf{X}} \in \mathbb{R}^{I_1 \times I_2 \times I_3}$ ,  $\underline{\mathbf{Y}} \in \mathbb{R}^{I_2 \times I_4 \times I_3}$   
**Output:** T-product  $\underline{\mathbf{C}} = \underline{\mathbf{X}} * \underline{\mathbf{Y}} \in \mathbb{R}^{I_1 \times I_4 \times I_3}$

- 1  $\widehat{\underline{\mathbf{X}}} = \text{fft}(\underline{\mathbf{X}}, [], 3);$
- 2  $\widehat{\underline{\mathbf{Y}}} = \text{fft}(\underline{\mathbf{Y}}, [], 3);$
- 3 **for**  $i = 1, 2, \dots, \lceil \frac{I_3+1}{2} \rceil$  **do**
- 4      $\widehat{\underline{\mathbf{C}}}(:, :, i) = \widehat{\underline{\mathbf{X}}}(:, :, i) \widehat{\underline{\mathbf{Y}}}(:, :, i);$
- 5 **end**
- 6 **for**  $i = \lceil \frac{I_3+1}{2} \rceil + 1 \dots, I_3$  **do**
- 7      $\widehat{\underline{\mathbf{C}}}(:, :, i) = \text{conj}(\widehat{\underline{\mathbf{C}}}(:, :, I_3 - i + 2));$
- 8 **end**
- 9  $\underline{\mathbf{C}} = \text{ifft}(\widehat{\underline{\mathbf{C}}}, [], 3);$

---

**Definition 2.** (Transpose) Let  $\underline{\mathbf{X}} \in \mathbb{R}^{I_1 \times I_2 \times I_3}$  be a given tensor. Then the transpose of the tensor  $\underline{\mathbf{X}}$  is denoted by  $\underline{\mathbf{X}}^T \in \mathbb{R}^{I_2 \times I_1 \times I_3}$ , which is constructed by transposing all its frontal slices and then reversing the order of transposed frontal slices 2 through  $I_3$ . A tensor  $\underline{\mathbf{X}} \in \mathbb{R}^{I \times I \times K}$  is called symmetric if  $\underline{\mathbf{X}}^T = \underline{\mathbf{X}}$ .

**Definition 3.** (Identity tensor) The tensor  $\underline{\mathbf{I}} \in \mathbb{R}^{I_1 \times I_1 \times I_3}$  is called identity if its first frontal slice is an identity matrix of size  $I_1 \times I_1$  and all other frontal slices are zero. It is easy to show  $\underline{\mathbf{I}} * \underline{\mathbf{X}} = \underline{\mathbf{X}}$  and  $\underline{\mathbf{X}} * \underline{\mathbf{I}} = \underline{\mathbf{X}}$  for all tensors of conforming sizes.

**Definition 4.** (Orthogonal tensor) A tensor  $\underline{\mathbf{X}} \in \mathbb{R}^{I_1 \times I_1 \times I_3}$  is orthogonal if  $\underline{\mathbf{X}}^T * \underline{\mathbf{X}} = \underline{\mathbf{X}} * \underline{\mathbf{X}}^T = \underline{\mathbf{I}}$ .

**Definition 5.** (Moore–Penrose pseudoinverse of a tensor) Let  $\underline{\mathbf{X}} \in \mathbb{R}^{I_1 \times I_2 \times I_3}$  be given. The Moore–Penrose (MP) pseudoinverse of the tensor  $\underline{\mathbf{X}}$  is denoted by  $\underline{\mathbf{X}}^\dagger \in \mathbb{R}^{I_2 \times I_1 \times I_3}$  is a unique tensor satisfying the following four equations:

$$\begin{aligned} \underline{\mathbf{X}}^\dagger * \underline{\mathbf{X}} * \underline{\mathbf{X}}^\dagger &= \underline{\mathbf{X}}^\dagger, & \underline{\mathbf{X}} * \underline{\mathbf{X}}^\dagger * \underline{\mathbf{X}} &= \underline{\mathbf{X}}, \\ (\underline{\mathbf{X}} * \underline{\mathbf{X}}^\dagger)^T &= \underline{\mathbf{X}} * \underline{\mathbf{X}}^\dagger, & (\underline{\mathbf{X}}^\dagger * \underline{\mathbf{X}})^T &= \underline{\mathbf{X}}^\dagger * \underline{\mathbf{X}}. \end{aligned}$$

The MP pseudoinverse of a tensor can also be computed in the Fourier domain and this is shown in Algorithm 2. The inverse of a tensor  $\underline{\mathbf{X}} \in \mathbb{R}^{I_1 \times I_1 \times I_3}$  is denoted by  $\underline{\mathbf{X}}^{\dagger} \in \mathbb{R}^{I_1 \times I_1 \times I_3}$  and is a special case of the MP for which we have  $\underline{\mathbf{X}}^{-1} * \underline{\mathbf{X}} = \underline{\mathbf{X}} * \underline{\mathbf{X}}^{-1} = \underline{\mathbf{I}}$ .

**Definition 6.** (f-diagonal tensor) If all frontal slices of a tensor are diagonal then the tensor is called an f-diagonal tensor.

**Definition 7.** (Random tensor) A tensor  $\underline{\mathbf{\Omega}}$  is random if its first frontal slice  $\underline{\mathbf{\Omega}}(:, :, 1)$  is a standard Gaussian matrix, while the other frontal slices are zero.

---

**Algorithm 2:** Fast Moore-Penrose pseudoinverse computation of the tensor  $\underline{\mathbf{X}}$

---

**Input :** The data tensor  $\underline{\mathbf{X}} \in \mathbb{R}^{I_1 \times I_2 \times I_3}$   
**Output:** Moore-Penrose pseudoinverse  $\underline{\mathbf{X}}^{\dagger} \in \mathbb{R}^{I_2 \times I_1 \times I_3}$

- 1  $\underline{\widehat{\mathbf{X}}} = \text{fft}(\underline{\mathbf{X}}, [], 3);$
- 2 **for**  $i = 1, 2, \dots, \lceil \frac{I_3+1}{2} \rceil$  **do**
- 3      $\underline{\widehat{\mathbf{C}}}(:, :, i) = \text{pinv}(\underline{\widehat{\mathbf{X}}}(:, :, i));$
- 4 **end**
- 5 **for**  $i = \lceil \frac{I_3+1}{2} \rceil + 1 \dots, I_3$  **do**
- 6      $\underline{\widehat{\mathbf{C}}}(:, :, i) = \text{conj}(\underline{\widehat{\mathbf{C}}}(:, :, I_3 - i + 2));$
- 7 **end**
- 8  $\underline{\mathbf{X}}^{\dagger} = \text{ifft}(\underline{\widehat{\mathbf{C}}}, [], 3);$

---

### 3. Generalization of standard matrix decomposition to tensors through the T-product

The T-product may be used to generalize standard matrix decompositions, such as QR, LU, eigenvalue decompositions and SVD, to tensors in a straightforward manner. Given a tensor  $\underline{\mathbf{X}} \in \mathbb{R}^{I_1 \times I_2 \times I_3}$ , the tensor QR (T-QR) represents a tensor in the form  $\underline{\mathbf{X}} = \underline{\mathbf{Q}} * \underline{\mathbf{R}}$  and can be computed through Algorithm 3. We use the notation “orth” for the operator to orthonormalize a given tensor (getting the  $\underline{\mathbf{Q}}$  part of the T-QR of a given tensor).

It is possible to calculate the tensor LU (T-LU), tensor eigenvalue decomposition (T-EIG) and tensor SVD (T-SVD) by slightly modifying Algorithm 3. More

specifically, we substitute the SVD, the LU decomposition and the eigenvalue decomposition of frontal slices  $\widehat{\mathbf{X}}(:, :, i)$ ,  $i = 1, 2, \dots, I_3$ , for the QR decomposition in line 4 of Algorithm 3. Please note that Algorithm 3 only needs the thin QR of the first  $\lceil \frac{I_3+1}{2} \rceil$  slices while the original T-QR algorithm developed in [31, 6] involves the QR of all frontal slices. So, it is recommended to utilize this idea and remove the redundant computations. For example, the T-QR decomposition for a symmetric tensor  $\mathbf{X} \in \mathbb{R}^{I_1 \times I_1 \times I_3}$  guarantees the following decomposition

$$\mathbf{X} = \mathbf{V} * \mathbf{D} * \mathbf{V}^T, \quad (3)$$

where  $\mathbf{D}$  is f-diagonal. The eigenvalue decomposition (3) can be also represented as follows

$$\mathbf{X} = (\mathbf{V} * \mathbf{D}^{1/2}) * (\mathbf{D}^{1/2} * \mathbf{V}^T), \quad (4)$$

where  $\mathbf{D}^{1/2} \equiv \text{sqrt}(\mathbf{D})$  is an f-diagonal tensor whose tubes are computed by performing the following computations on each tube of the f-diagonal tensor  $\mathbf{D}$ , say  $\mathbf{D}(i, i, :)$ .

---

```

1  $\widehat{\mathbf{D}}(i, i, :) = \text{fft}(\mathbf{D}(i, i, :), [], 3);$ 
2 for  $j = 1 : I_3$  do
3   |  $\widehat{\mathbf{D}}(i, i, j) = \text{sqrt}(\widehat{\mathbf{D}}(i, i, j));$ 
4 end
5  $\mathbf{D}^{1/2}(i, i, :) = \text{ifft}(\widehat{\mathbf{D}}(i, i, :), [], 3);$ 

```

---

It is worth to also note that the T-SVD is a useful tensor decomposition, which represent a tensor as the T-product of three tensors. The first and last tensors are orthogonal while the middle tensor is f-diagonal. Let  $\mathbf{X} \in \mathbb{R}^{I_1 \times I_2 \times I_3}$  be a tensor, then the T-SVD of this tensor is represented as follows

$$\mathbf{X} = \mathbf{U} * \mathbf{S} * \mathbf{V}^T, \quad (5)$$

where  $\mathbf{U} \in \mathbb{R}^{I_1 \times I_1 \times I_3}$  and  $\mathbf{V} \in \mathbb{R}^{I_2 \times I_2 \times I_3}$  are orthogonal, while  $\mathbf{S} \in \mathbb{R}^{I_1 \times I_2 \times I_3}$  is f-diagonal. The number of non-zero diagonal tubes of the the tensor  $\mathbf{S} \in \mathbb{R}^{I_1 \times I_2 \times I_3}$  is called the tubal rank. The truncated T-SVD is defined by truncating the tensors  $\mathbf{U}$ ,  $\mathbf{S}$ , and  $\mathbf{V}$ . For example a truncated T-SVD of tubal rank  $R$  for the tensor  $\mathbf{X}$  is

$$\mathbf{X} \approx \mathbf{U}_R * \mathbf{S}_R * \mathbf{V}_R^T, \quad (6)$$

where  $\mathbf{U}_R = \mathbf{U}(1 : R, :, :) \in \mathbb{R}^{I_1 \times R \times I_3}$ ,  $\mathbf{V}_R = \mathbf{V}(:, 1 : R, :) \in \mathbb{R}^{R \times I_2 \times I_3}$ , and  $\mathbf{S}_R = \mathbf{S}(1 : R, 1 : R, :) \in \mathbb{R}^{R \times R \times I_3}$ . Figure 2 illustrates the structure of this decomposition and its truncated version.



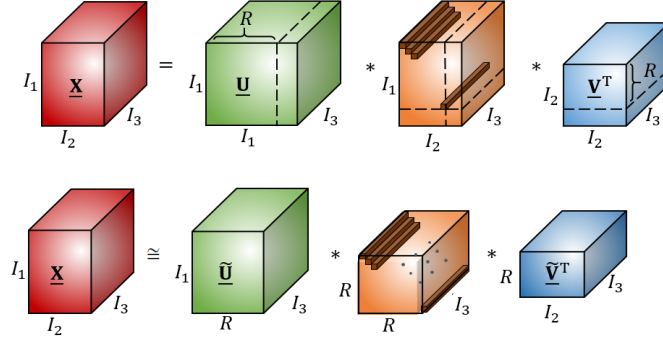


Figure 2: Illustration of (a) Tensor SVD (T-SVD) and (b) truncated T-SVD for a third-order tensor .

---

**Algorithm 3:** Fast T-QR decomposition of the tensor  $\underline{\mathbf{X}}$

---

**Input :** The data tensor  $\underline{\mathbf{X}} \in \mathbb{R}^{I_1 \times I_2 \times I_3}$

**Output:** The T-QR computation  $\underline{\mathbf{X}} = \underline{\mathbf{Q}} * \underline{\mathbf{R}}$ .

- 1  $\widehat{\underline{\mathbf{X}}} = \text{fft}(\underline{\mathbf{X}}, [], 3)$ ;
  - 2 **for**  $i = 1, 2, \dots, \lceil \frac{I_3+1}{2} \rceil$  **do**
  - 3      $[\widehat{\underline{\mathbf{Q}}}(:, :, i), \widehat{\underline{\mathbf{R}}}(:, :, i)] = \text{qr}(\widehat{\underline{\mathbf{X}}}(:, :, i), 0)$ ;
  - 4 **end**
  - 5 **for**  $i = \lceil \frac{I_3+1}{2} \rceil + 1 \dots, I_3$  **do**
  - 6      $\widehat{\underline{\mathbf{Q}}}(:, :, i) = \text{conj}(\widehat{\underline{\mathbf{C}}}(:, :, I_3 - i + 2))$ ;
  - 7      $\widehat{\underline{\mathbf{R}}}(:, :, i) = \text{conj}(\widehat{\underline{\mathbf{R}}}(:, :, I_3 - i + 2))$ ;
  - 8 **end**
  - 9  $\underline{\mathbf{Q}} = \text{ifft}(\widehat{\underline{\mathbf{Q}}}, [], 3)$ ;
  - 10  $\underline{\mathbf{R}} = \text{ifft}(\widehat{\underline{\mathbf{R}}}, [], 3)$ ;
-

#### 4. Proposed randomized single-pass algorithms

Randomized single-pass algorithms are a class of algorithms that process a stream of data in a single pass and do not need to store the entire dataset in memory, which is crucial for large datasets that cannot fit in memory. They play a vital role in processing massive datasets and providing efficient solutions in various applications. Their ability to process data in a single pass, reduce memory usage, and handle worst-case scenarios makes them essential for real-time data analysis, data streaming, and machine learning tasks. Because of these reasons, developing single-pass and, in general, pass-efficient algorithms for fast low tensor rank approximation has been a hot topic in the last decade.

In this paper, we focus on the T-SVD and propose new single-pass algorithms. To the best of our knowledge, the only single-pass algorithms proposed for low tubal rank approximation of tensors were proposed in [37] and [32]. The proposed approach in [37] is based on the cross tensor approximation, that is, for a given tensor  $\underline{\mathbf{X}} \in \mathbb{R}^{I_1 \times I_2 \times I_3}$ , a low tubal rank approximation computed by sampling some lateral and horizontal slices of the original data tensor  $\underline{\mathbf{X}}$ , see Figure 1 for an illustration. So, if  $\underline{\mathbf{C}} \in \mathbb{R}^{I_1 \times L \times I_3}$  and  $\underline{\mathbf{R}} \in \mathbb{R}^{K \times I_2 \times I_3}$  are some selected lateral and horizontal slices<sup>2</sup> of the data tensor  $\underline{\mathbf{X}}$ . Then, a low tubal rank approximation is computed as follows

$$\underline{\mathbf{X}} \approx \underline{\mathbf{C}} * \underline{\mathbf{U}} * \underline{\mathbf{R}}, \quad (7)$$

where  $\underline{\mathbf{U}} = \underline{\mathbf{C}}^\dagger * \underline{\mathbf{X}} * \underline{\mathbf{R}}^\dagger$ . The middle tensor  $\underline{\mathbf{U}}$  is the best candidate as it minimizes the residual  $\|\underline{\mathbf{X}} - \underline{\mathbf{C}} * \underline{\mathbf{U}} * \underline{\mathbf{R}}\|_F$ . Obviously, this approach requires only one pass over the data for computing the middle tensor  $\underline{\mathbf{U}}$ . Our experimental results confirm that this method is stable in the sense of a number of lateral and horizontal slice selections, but this approach has three main drawbacks. First, its accuracy is usually less than other techniques because the factor tensors  $\underline{\mathbf{C}}$  and  $\underline{\mathbf{R}}$  are not very accurate estimates of left and right singular tensors. Secondly, it usually requires a larger tubal rank for the desired accuracy. Thirdly, the computation of  $\underline{\mathbf{C}}^\dagger * \underline{\mathbf{X}} * \underline{\mathbf{R}}^\dagger$  is more expensive than the case of multiplication with random tensors because one can use structured random tensors to speed up the computations. In [37], it is suggested to use  $\underline{\mathbf{U}}$  as the intersection tensor of some selected lateral and horizontal slices, as shown in Figure 1. This new method is quite fast but suffers from the same instability problem when  $L = K$ , that is the number of lateral slices

---

<sup>2</sup>Please note that it is not necessary the number of lateral and frontal slices be of the same size.

is the same as the number of horizontal slices. This algorithm is summarized in Algorithm 4.

The single-pass method proposed in [32], is a generalization of the single-pass matrix algorithm [35] to the tensor case. To be more precise, let  $\underline{\mathbf{X}} \in \mathbb{R}^{I_1 \times I_2 \times I_3}$  be given. Then, in the first step, two sketches are computed from  $\underline{\mathbf{X}}$  by multiplying it with two random tensors  $\underline{\Omega}_1 \in \mathbb{R}^{I_2 \times K \times I_3}$  and  $\underline{\Omega}_2 \in \mathbb{R}^{L \times I_1 \times I_3}$ , ( $K \leq L$ ) as follows:

$$\underline{\mathbf{Y}} = \underline{\mathbf{X}} * \underline{\Omega}_1 \in \mathbb{R}^{I_1 \times K \times I_3}, \quad \underline{\mathbf{W}} = \underline{\Omega}_2 * \underline{\mathbf{X}} \in \mathbb{R}^{L \times I_2 \times I_3}. \quad (8)$$

Suppose that  $\underline{\mathbf{Q}} \in \mathbb{R}^{I_1 \times K \times I_3}$  is an orthonormal basis for the range of the tensor  $\underline{\mathbf{Y}}$ , computed by the T-QR algorithm, and a low tubal rank approximation is computed as

$$\underline{\mathbf{X}} \approx \underline{\mathbf{Q}} * (\underline{\mathbf{Q}}^T * \underline{\mathbf{X}}). \quad (9)$$

Here,  $L$  and  $K$  are called sketch sizes, and  $\underline{\mathbf{Y}}$  or  $\underline{\mathbf{W}}$  are called sketches of the tensor  $\underline{\mathbf{X}}$ . However, since it (8), we passed the data tensor once, we should avoid computing  $\underline{\mathbf{Q}}^T * \underline{\mathbf{X}}$  in (9) again because it requires us to view the original data  $\underline{\mathbf{X}}$  one more time. This can be actually estimated as follows

$$\underline{\mathbf{Q}}^T * \underline{\mathbf{X}} \approx (\underline{\Omega}_2 * \underline{\mathbf{Q}})^\dagger * \underline{\mathbf{W}}. \quad (10)$$

So, this single-pass or 1-view method combines range and co-range sketches in a single pass over the data tensor  $\underline{\mathbf{X}}$ , and then generate a low tubal rank estimate based on information included in the sketches. These algorithms is summarized in Algorithms 5. Consider a streaming setting where the data tensor  $\underline{\mathbf{X}}$  is never entirely kept in random-access memory but is instead given as a finite stream of linear updates.

$$\underline{\mathbf{X}} = \sum_{n=1}^N \underline{\mathbf{H}}_n.$$

Here, each  $\underline{\mathbf{H}}_n$  is deleted once it is used, and we can gradually sample from  $\underline{\mathbf{X}}$  as each innovation tensor  $\underline{\mathbf{H}}_n$  is provided as follows.

$$\underline{\mathbf{X}} * \underline{\Omega}_1 = \sum_{i=n}^N \underline{\mathbf{H}}_n * \underline{\Omega}_1, \quad \underline{\Omega}_2 * \underline{\mathbf{X}} = \sum_{n=1}^N \underline{\Omega}_2 * \underline{\mathbf{H}}_n.$$

This is an example where single-pass algorithms are applicable because each  $\underline{\mathbf{H}}_n$  could represent a sparse tensor containing a few elements of  $\underline{\mathbf{X}}$ .

As discussed in [36], the single-pass algorithms for matrices usually give unreliable approximations when  $L = K$  due to some instability issues in solving badly conditioned least-squares problems. Actually, we experienced the same for tensors and will report them in our simulations. According to (10), we need to solve the linear tensor equation  $(\underline{\Omega}_2 * \underline{\mathbf{Q}}) * \underline{\mathbf{Y}} = \underline{\mathbf{W}}$ . The coefficient tensor  $\underline{\Omega}_2 * \underline{\mathbf{Q}} \in \mathbb{R}^{L \times K \times I_3}$  has  $L$  and  $K$  number of horizontal and lateral slices, respectively. One way to avoid the badly conditioned coefficient tensor is considering  $L > K$  and solving an overdetermined and better-conditioned problem. However, this requires fine-tuning the parameters  $L$  and  $K$  to get an acceptable approximation, imposing extra costs of carefully identifying the best of such values, otherwise there is a the risk of losing accuracy. On the other hand, as highlighted in [36], one other reason to address the disadvantages of selecting  $L = K$  is that  $K$  may represent a processing bottleneck in some applications. Given the computing limitations, it would thus be tempting to set  $L = K$  in an attempt to obtain as much information as possible. Nevertheless, the requirement to retain both the sketching and random sample matrices places a memory restriction on the 1-view approach. The last comment that needs to be mentioned is that using prior information from the singular values of the matrix at hand in [35], several ways are suggested to select  $L$  and  $K$ , which are of less practical interest when we have no access to such information. It is worth mentioning that in all our proposed single-pass algorithms, the sketches  $\underline{\mathbf{Y}}_c$  or  $\underline{\mathbf{Y}}_r$  are much smaller than the original data tensor, and computing their left singular vectors will not be very expensive compared to only an orthonormal basis for the range sketch. Particularly since, in single-pass techniques, multiplying  $\underline{\mathbf{X}}$  to random tensors (to discover range and co-range sketches) usually imposes the most computational cost and time.

To overcome this drawback, more stabilized and improved algorithms (see Algorithms 7 and 8 in [36]) were developed in [36] for matrices. Motivated by their efficiency, we generalized them to the tensor case and are summarized in Algorithms 6 and 7. The principal idea is to use the truncated T-SVD for getting an orthonormal basis for the full range of the sketches  $\underline{\mathbf{Y}}_r$  or  $\underline{\mathbf{Y}}_c$  instead of applying the T-QR decomposition. Let us explain this in detail. Instead of considering  $\underline{\mathbf{Q}}$  as an orthonormal basis for  $\underline{\mathbf{Y}}$ , we compute  $[\underline{\mathbf{Q}}, \sim, \sim] = \text{Truncated T-SVD}(\underline{\mathbf{Y}}, \overline{H})$ , where  $0 \leq H \leq K$ . This means that  $\underline{\mathbf{Q}} \in \mathbb{R}^{I_1 \times H \times I_3}$  contains the leading left singular tensors of  $\underline{\mathbf{Y}}$ , and if  $H \leq K$ , then coefficient tensor  $\underline{\Omega}_2 * \underline{\mathbf{Q}} \in \mathbb{R}^{L \times H \times I_3}$  should provide a more conditioned problem, even for  $L = K$ .

Note that other single-pass methods, such as two-sided randomized SVD (TSR-SVD) [41], can also be extended to the tensor case. The TSR-SVD uses the com-

pressed tensor  $\underline{\mathbf{W}} = \underline{\Omega}_2 * \underline{\mathbf{X}} * \underline{\Omega}_1$ , where  $\underline{\Omega}_1$  and  $\underline{\Omega}_2$  are standard Gaussian tensors of conforming sizes, to compute a low tubal rank approximation of a tensor. To be more precise, for a data tensor  $\underline{\mathbf{X}}$ , and orthogonal bases  $\underline{\mathbf{Q}}_1$  and  $\underline{\mathbf{Q}}_2$ , we have

$$\underline{\mathbf{X}} \approx \underline{\mathbf{Q}}_1 * \left( \underline{\mathbf{Q}}_1^T * \underline{\mathbf{X}} * \underline{\mathbf{Q}}_2 \right) * \underline{\mathbf{Q}}_2^T. \quad (11)$$

It is not difficult to see that the middle tensor in (11), can be approximated as follows

$$\underline{\mathbf{Q}}_1^T * \underline{\mathbf{X}} * \underline{\mathbf{Q}}_2 \approx (\underline{\Omega}_2 * \underline{\mathbf{Q}})^\dagger * \underline{\mathbf{W}} * (\underline{\mathbf{Q}}^T * \underline{\Omega}_1)^\dagger, \quad (12)$$

and

$$\underline{\mathbf{Q}}_1^T * \underline{\mathbf{X}} * \underline{\mathbf{Q}}_2 \approx (\underline{\mathbf{Q}}_1^T * \underline{\mathbf{Y}}) * (\underline{\mathbf{Q}}_2 * \underline{\Omega}_1)^\dagger, \quad (13)$$

Both of these require one to pass over the underlying data matrix.

These algorithms are also not stable for  $L = K$ . In our simulations, both of them provided similar results, and due to this issue, we only report for the formulation (13). We first extended the TSR-SVD algorithm to the tensor case, and we refer to it as the TSRT-SVD algorithm. We also stabilize it to work for  $L = K$ . It is summarized in Algorithm 8. It is clear that Algorithms 6, 7, and 8 pass the original data tensor only once at the beginning of the algorithm (Line 2). This Line can be performed in parallel. It is suggested in [35] to orthonormalize the random tensors in Line 1 in the single-pass algorithms when a large oversampling parameter is used, which can be naturally extended to the tensor case. We have not tried this idea in our experiments.

---

**Algorithm 4:** The single-pass cross tensor approximation [37]

---

**Input :** The data tensor  $\underline{\mathbf{X}} \in \mathbb{R}^{I_1 \times I_2 \times I_3}$ , two parameters  $L, K$

**Output:** A low tubal rank approximation  $\underline{\mathbf{X}} \approx \underline{\mathbf{C}} * \underline{\mathbf{U}} * \underline{\mathbf{R}}$

- 1 Select  $L$  lateral slices  $\underline{\mathbf{C}}$  with corresponding indices  $\mathcal{L}$ ;
  - 2 Select  $K$  horizontal slices  $\underline{\mathbf{R}}$  with corresponding indices  $\mathcal{K}$ ;
  - 3 Construct the intersection tensor  $\underline{\mathbf{W}} = \underline{\mathbf{X}}(\mathcal{L}, \mathcal{K}, :)$ ;
  - 4 Compute the middle tensor  $\underline{\mathbf{U}} = \underline{\mathbf{W}}^\dagger$ ;
  - 5 Compute a low tubal rank approximation  $\underline{\mathbf{X}} \approx \underline{\mathbf{C}} * \underline{\mathbf{U}} * \underline{\mathbf{R}}$ ;
-

---

**Algorithm 5:** The Single-pass algorithm proposed in [32]

---

**Input :** The data tensor  $\underline{\mathbf{X}} \in \mathbb{R}^{I_1 \times I_2 \times I_3}$ , two parameters  $L, K$

**Output:** A low tubal rank approximation  $\underline{\mathbf{X}} \approx \underline{\mathbf{Q}} * \underline{\mathbf{B}}$

- 1  $\underline{\Omega}_1 = \text{randn}(I_2, K, I_3)$ ,  $\underline{\Omega}_2 = \text{randn}(L, I_1, I_3)$ ;
  - 2 Compute two sketches:  
 $\underline{\mathbf{Y}} = \underline{\mathbf{X}} * \underline{\Omega}_1 \in \mathbb{R}^{I_1 \times K \times I_3}$ ,  $\underline{\mathbf{W}} = \underline{\Omega}_2 * \underline{\mathbf{X}} \in \mathbb{R}^{L \times I_2 \times I_3}$ ;
  - 3 Apply the T-QR applied to  $\underline{\mathbf{Y}}$  and obtain the tensor  $\underline{\mathbf{Q}}$ ;
  - 4 Compute the tensor  $\underline{\mathbf{B}} = (\underline{\Gamma} * \underline{\mathbf{Q}})^\dagger * \underline{\mathbf{W}}$ ;
  - 5 Compute the low tubal rank approximation  $\underline{\mathbf{X}} \approx \underline{\mathbf{Q}} * \underline{\mathbf{B}}$ ;
- 

---

**Algorithm 6:** Proposed randomized single-pass algorithm I

---

**Input :** The data tensor  $\underline{\mathbf{X}} \in \mathbb{R}^{I_1 \times I_2 \times I_3}$ , three parameters  $L, K, H$ ,  
 $L \geq K \geq H \geq 0$  and a target tubal rank  $R$

**Output:** A low tubal rank approximation  $\underline{\mathbf{X}} \approx \underline{\mathbf{U}} * \underline{\mathbf{S}} * \underline{\mathbf{V}}^T$

- 1  $\underline{\Omega}_1 = \text{randn}(I_2, K, I_3)$ ,  $\underline{\Omega}_2 = \text{randn}(I_1, L, I_3)$ ;
  - 2  $\underline{\mathbf{Y}}_c = \underline{\mathbf{X}} * \underline{\Omega}_1$ ,  $\underline{\mathbf{Y}}_r = \underline{\mathbf{X}}^T * \underline{\Omega}_2$ ;
  - 3 **if**  $H < K$  **then**
  - 4      $[\underline{\mathbf{Q}}_c, \underline{\mathbf{R}}_c] = \text{T-QR}(\underline{\mathbf{Y}}_c)$ ;
  - 5      $[\hat{\underline{\mathbf{Q}}}_c, \sim, \sim] = \text{Truncated T-SVD}(\underline{\mathbf{R}}_c, R + H)$ ;
  - 6      $\underline{\mathbf{Q}}_c = \underline{\mathbf{Q}}_c * \hat{\underline{\mathbf{Q}}}_c$ ;
  - 7 **else**
  - 8      $[\underline{\mathbf{Q}}_c, \sim] = \text{T-QR}(\underline{\mathbf{Y}}_c)$ ;
  - 9 **end**
  - 10  $[\hat{\underline{\mathbf{Q}}}, \hat{\underline{\mathbf{R}}}] = \text{T-QR}(\underline{\Omega}_2^T * \underline{\mathbf{Q}}_c)$ ;
  - 11  $\underline{\mathbf{Z}} = \hat{\underline{\mathbf{R}}}^{-1} * \hat{\underline{\mathbf{Q}}} * \underline{\mathbf{Y}}_r^T$ ;
  - 12  $[\tilde{\underline{\mathbf{U}}}, \underline{\mathbf{S}}, \underline{\mathbf{V}}] = \text{Truncated T-SVD}(\underline{\mathbf{Z}}, R)$ ;
  - 13  $\underline{\mathbf{U}} = \underline{\mathbf{Q}} * \hat{\underline{\mathbf{U}}}$ ;
-

---

**Algorithm 7:** Proposed randomized single-pass algorithm II
 

---

**Input :** The data tensor  $\underline{\mathbf{X}} \in \mathbb{R}^{I_1 \times I_2 \times I_3}$ , three parameters  $L, K, H$ ,  
 $L \geq K \geq H \geq 0$  and a target tubal rank  $R$ .

**Output:** A low tubal rank approximation  $\underline{\mathbf{X}} \approx \underline{\mathbf{U}} * \underline{\mathbf{S}} * \underline{\mathbf{V}}^T$

- 1  $\underline{\mathbf{\Omega}}_1 = \text{randn}(I_2, K, I_3)$ ,  $\underline{\mathbf{\Omega}}_2 = \text{randn}(I_1, L, I_3)$ ;
  - 2  $\underline{\mathbf{Y}}_c = \underline{\mathbf{X}} * \underline{\mathbf{\Omega}}_1$ ,  $\underline{\mathbf{Y}}_r = \underline{\mathbf{X}}^T * \underline{\mathbf{\Omega}}_2$ ;
  - 3  $[\underline{\mathbf{Q}}_c, \underline{\mathbf{R}}_c] = \text{T-QR}(\underline{\mathbf{Y}}_c)$ ;
  - 4  $[\underline{\mathbf{Q}}_r, \underline{\mathbf{R}}_r] = \text{T-QR}(\underline{\mathbf{Y}}_r)$ ;
  - 5  $[\tilde{\underline{\mathbf{Q}}}_c, \sim, \sim] = \text{Truncated T-SVD}(\underline{\mathbf{R}}_c, R + H)$ ;
  - 6  $[\tilde{\underline{\mathbf{Q}}}_r, \sim, \sim] = \text{Truncated T-SVD}(\underline{\mathbf{R}}_r, R + H)$ ;
  - 7  $\underline{\mathbf{Q}}_c = \underline{\mathbf{Q}}_c * \tilde{\underline{\mathbf{Q}}}_c$ ;
  - 8  $\underline{\mathbf{Q}}_r = \underline{\mathbf{Q}}_r * \tilde{\underline{\mathbf{Q}}}_r$ ;
  - 9  $\hat{\underline{\mathbf{Z}}} = (\underline{\mathbf{\Omega}}_2^T * \underline{\mathbf{Q}}_c)^\dagger * (\underline{\mathbf{Y}}_r^T * \underline{\mathbf{Q}}_r)$ ;
  - 10  $[\tilde{\underline{\mathbf{U}}}, \tilde{\underline{\mathbf{S}}}, \tilde{\underline{\mathbf{V}}}] = \text{Truncated T-SVD}(\hat{\underline{\mathbf{Z}}}, R)$ ;
  - 11  $\underline{\mathbf{U}} = \underline{\mathbf{Q}}_c * \tilde{\underline{\mathbf{U}}}$ ;
  - 12  $\underline{\mathbf{V}} = \underline{\mathbf{Q}}_r * \tilde{\underline{\mathbf{V}}}$ ;
-

---

**Algorithm 8:** Proposed randomized single-pass (two-sided version) algorithm III

---

**Input :** The data tensor  $\underline{\mathbf{X}} \in \mathbb{R}^{I_1 \times I_2 \times I_3}$ , three parameters  $L, K, H$ ,  
 $L \geq K \geq H \geq 0$  and a target tubal rank  $R$

**Output:** A low tubal rank approximation  $\underline{\mathbf{X}} \approx \underline{\mathbf{U}} * \underline{\mathbf{S}} * \underline{\mathbf{V}}^T$

- 1  $\underline{\Omega}_1 = \text{randn}(I_2, K, I_3)$ ,  $\underline{\Omega}_2 = \text{randn}(I_1, L, I_3)$ ;
  - 2  $\underline{\mathbf{Y}}_c = \underline{\mathbf{X}} * \underline{\Omega}_1$ ,  $\underline{\mathbf{Y}}_r = \underline{\mathbf{X}}^T * \underline{\Omega}_2$ ;
  - 3  $[\underline{\mathbf{Q}}_c, \underline{\mathbf{R}}_c] = \text{T-QR}(\underline{\mathbf{Y}}_c)$ ;
  - 4  $[\underline{\mathbf{Q}}_r, \underline{\mathbf{R}}_r] = \text{T-QR}(\underline{\mathbf{Y}}_r)$ ;
  - 5  $[\tilde{\underline{\mathbf{Q}}}_c, \sim, \sim] = \text{Truncated T-SVD}(\underline{\mathbf{R}}_c, R + H)$ ;
  - 6  $[\tilde{\underline{\mathbf{Q}}}_r, \sim, \sim] = \text{Truncated T-SVD}(\underline{\mathbf{R}}_r, R + H)$ ;
  - 7  $\underline{\mathbf{Q}}_c = \underline{\mathbf{Q}}_c * \tilde{\underline{\mathbf{Q}}}_c$ ;
  - 8  $\underline{\mathbf{Q}}_r = \underline{\mathbf{Q}}_r * \tilde{\underline{\mathbf{Q}}}_r$ ;
  - 9  $\underline{\mathbf{B}} = \underline{\mathbf{Q}}_c^T * \underline{\mathbf{Y}}_c * (\underline{\mathbf{Q}}_r^T * \underline{\Omega}_1)^\dagger$ ;
  - 10  $[\tilde{\underline{\mathbf{U}}}, \tilde{\underline{\mathbf{S}}}, \tilde{\underline{\mathbf{V}}}] = \text{Truncated T-SVD}(\underline{\mathbf{B}}, R)$ ;
  - 11  $\underline{\mathbf{U}} = \underline{\mathbf{Q}}_c * \tilde{\underline{\mathbf{U}}}$ ;
  - 12  $\underline{\mathbf{V}} = \underline{\mathbf{Q}}_r * \tilde{\underline{\mathbf{V}}}$ ;
-



## 5. Proposed randomized fixed-precision algorithms

Randomized fixed-precision algorithms for tensors are referred to as algorithms that can automatically estimate an appropriate/optimal tensor rank and the corresponding low-rank tensor approximation. These algorithms have crucial applications when we have no knowledge about the data’s rank or when estimating it is difficult. In such scenarios, one needs to estimate the optimal rank and the corresponding low tubal rank approximation for a prescribed error approximation bound.

We have recently developed a randomized fixed-precision algorithm [38], and simulations on synthetic and real-world data showed a significant acceleration in the computation of approximate truncated T-SVD. Our work was a generalization of the matrix case [42] to the tensor case. This algorithm is presented in Algorithm 9. The algorithm requires an oversampling, a power iteration, a tolerance, and a block size, and it gradually estimates the tubal rank and computes the corresponding low tubal rank approximation. Lines 6-9 are the power iteration stage for achieving better accuracy, especially when the singular values of the frontal slices of the data tensor dot have a fast decaying rate.

However, recently, the matrix version of this algorithm was further improved in [39] and [43]. Motivated by the interesting results reported in that paper, we enhance our previously randomized fixed-precision algorithm. We improve our proposed algorithm in [38] in several ways. First of all, for a given power iteration, Algorithm 9 requires  $2q + 2$  to pass over the original data tensor at each iteration of the algorithm. This means that for a given power iteration, we are forced to view the original data, even the number of passes. Clearly, this is a limitation, as we have shown in [33], for example, for the case of images or videos, usually three passes are sufficient for getting satisfying results. However, Algorithm 9 does not allow three passes, and for  $q = 2$ , we will have 4 passes, and this additional pass could be expensive for very large-scale data tensors or if the underlying algorithm requires many iterations for the convergence. Indeed, we aim at improving Algorithm 9, and our new proposed method summarized in Algorithm 10 addresses this problem. A given error bound can provide an estimation of the tubal rank and a low tubal rank approximation for any number of passes. Please note that in Algorithm 9,  $q$  is the power iteration parameter while  $q$  is the number of passes in Algorithm 10. Similar to [43], we do the following modifications to algorithm 9 to be more pass-efficient

- Employing the T-EIG decomposition for computing the truncated T-SVD of **B**.

- Ignoring one orthonormalization process in each round of the power iteration loop.
- Replacing the T-LU decomposition instead of T-QR for the orthonormalization process in the power iteration (except the last round of the iteration).
- Modifying the algorithm to allow an odd number of passes.

It is worth noting that in Algorithm 10, we consider the tail of tensor factors  $\widehat{\mathbf{U}}$ ,  $\widehat{\mathbf{V}}$ ,  $\widehat{\mathbf{S}}$  in lines 26-27 since the eigenvalue decomposition of symmetric matrices is computed in ascending order using the MATLAB function “eig”. Algorithm 9 can also be improved in terms of replacing the T-QR decomposition (orthonormalization step) with T-product and the tensor inverse of small tensors because it is known that QR decomposition is a key operation in the T-QR decomposition a comparatively low efficiency in multi-threaded computing. Following the idea proposed in [39], we replace this operation with the T-product of tensors and the inversion of small tensors, whose capacity for parallelization is superior. This algorithm is summarized in Algorithm 11, and we describe it in the sequel.

**Theorem 1.** Let  $\underline{\mathbf{X}} \in \mathbb{R}^{I_1 \times I_2 \times I_3}$  and  $\underline{\mathbf{\Omega}} \in \mathbb{R}^{I_2 \times k \times I_3}$  be a random tensor  $\underline{\mathbf{Y}} = \underline{\mathbf{X}} * \underline{\mathbf{\Omega}}$ ,  $\underline{\mathbf{W}} = \underline{\mathbf{X}}^T * \underline{\mathbf{Y}}$  and the economic T-SVD of  $\underline{\mathbf{Y}}$  is  $\underline{\mathbf{Y}} = \widehat{\mathbf{U}} * \widehat{\mathbf{S}} * \widehat{\mathbf{V}}^T$ . Setting

$$\underline{\mathbf{Q}} = \underline{\mathbf{Y}} * \widehat{\mathbf{V}} * \widehat{\mathbf{S}}^{-1}, \quad \underline{\mathbf{B}} = (\underline{\mathbf{W}} * \widehat{\mathbf{V}} * \widehat{\mathbf{S}}^{-1})^T, \quad (14)$$

gives an approximation  $\underline{\mathbf{Q}} * \underline{\mathbf{B}}$  to  $\underline{\mathbf{X}}$  that has the same accuracy of ... and

$$\|\underline{\mathbf{B}}\|_F^2 = \text{trace}(\underline{\mathbf{H}}_1),$$

where  $\underline{\mathbf{H}}_1 = \underline{\mathbf{H}}(:, :, 1)$  is the first frontal slice of  $\underline{\mathbf{H}} = \underline{\mathbf{W}} * \underline{\mathbf{W}}^T * (\underline{\mathbf{Y}} * \underline{\mathbf{Y}})^{-1}$ .

*Proof.* The proof of this theorem is very similar to the Proposition 1 in [39]. Considering the following identities

$$\underline{\mathbf{Q}} = \text{orth}(\underline{\mathbf{X}} * \underline{\mathbf{\Omega}}) = \text{orth}(\underline{\mathbf{Y}}) = \widehat{\mathbf{U}} = \underline{\mathbf{Y}} * \widehat{\mathbf{V}} * \widehat{\mathbf{S}}^{-1}, \quad (15)$$

and substituting (15) in  $\underline{\mathbf{B}} = \underline{\mathbf{Q}}^T * \underline{\mathbf{X}}$ , we have

$$\underline{\mathbf{B}} \equiv \underline{\mathbf{Q}}^T * \underline{\mathbf{X}} = (\underline{\mathbf{W}} * \widehat{\mathbf{V}} * \widehat{\mathbf{S}})^T. \quad (16)$$

Now, using the fact that  $\|\underline{\mathbf{B}}\|_F^2 = \text{trace}(\underline{\mathbf{G}}_1) = \underline{\mathbf{G}}(:, :, 1)$  where  $\underline{\mathbf{G}}_1$  is the first frontal slice of  $\underline{\mathbf{G}} = \underline{\mathbf{B}}^T * \underline{\mathbf{B}}$ , we have

$$\begin{aligned} \|\underline{\mathbf{B}}\|_F^2 &= \text{trace}(\underline{\mathbf{G}}_1) = \text{trace}((\widehat{\mathbf{S}}^{-1} * \widehat{\mathbf{V}}^T * \underline{\mathbf{W}}^T * \underline{\mathbf{W}} * \widehat{\mathbf{V}} * \widehat{\mathbf{S}}^{-1})_1) \\ &= \text{trace}((\underline{\mathbf{W}}^T * \underline{\mathbf{W}} * \widehat{\mathbf{V}} * \widehat{\mathbf{S}}^{-2} * \widehat{\mathbf{V}}^T)_1) \\ &= \text{trace}((\underline{\mathbf{W}}^T * \underline{\mathbf{W}} * (\underline{\mathbf{Y}}^T * \underline{\mathbf{Y}})^{-1})_1). \end{aligned} \quad (17)$$

This proves the theorem.  $\square$

From Theorem 1 and defining  $\underline{\mathbf{T}} = \underline{\mathbf{W}}^T * \underline{\mathbf{W}}$  and  $\underline{\mathbf{Z}} = \underline{\mathbf{Y}}^T * \underline{\mathbf{Y}}$ , the stopping criterion  $\|\underline{\mathbf{X}} - \underline{\mathbf{Q}} * \underline{\mathbf{B}}\|_F^2 = \|\underline{\mathbf{Q}}\|_F^2 - \|\underline{\mathbf{B}}\|_F^2$  can be reduced to

$$\|\underline{\mathbf{X}} - \underline{\mathbf{Q}} * \underline{\mathbf{B}}\|_F^2 = \|\underline{\mathbf{Q}}\|_F^2 - \text{trace}((\underline{\mathbf{T}} * \underline{\mathbf{Z}}^{-1})_1),$$

which is used in Algorithm 11 in Line 13. From Theorem 1, it is also follows that

$$\underline{\mathbf{Q}} * \underline{\mathbf{B}} = \underline{\mathbf{Y}} * \widehat{\mathbf{V}} * \widehat{\mathbf{S}}^{-2} * \widehat{\mathbf{V}}^T * \underline{\mathbf{W}}^T = \underline{\mathbf{Y}} * (\underline{\mathbf{Y}}^T * \underline{\mathbf{Y}})^{-1} * \underline{\mathbf{W}}^T, \quad (18)$$

so,  $\underline{\mathbf{Q}} * \underline{\mathbf{B}} = \underline{\mathbf{Y}} * \underline{\mathbf{Z}}^{-1} * \underline{\mathbf{W}}^T$ . This illustrates that the power iteration in Algorithm 9 can be replaced with  $\underline{\mathbf{X}} - \underline{\mathbf{Y}} * \underline{\mathbf{Z}}^{-1} * \underline{\mathbf{W}}^T$ . That is, Lines 6-9 in Algorithm 9 can be replaced by the following computations

---



---

```

1 for  $j = 1 : p$  do
2    $\underline{\mathbf{Y}}_i \leftarrow \underline{\mathbf{X}} * \underline{\mathbf{\Omega}}_i - \underline{\mathbf{Y}} * \underline{\mathbf{Z}}^{-1} * \underline{\mathbf{W}}^T * \underline{\mathbf{\Omega}}_i;$ 
3    $\underline{\mathbf{W}}_i \leftarrow \underline{\mathbf{X}}^T * \underline{\mathbf{Y}}_i - \underline{\mathbf{W}} * \underline{\mathbf{Z}}^{-1} * \underline{\mathbf{Y}}^T * \underline{\mathbf{Y}}_i;$ 
4    $\underline{\mathbf{\Omega}}_i \leftarrow \text{orth}(\underline{\mathbf{W}}_i)$ 
5 end

```

---

Substituting Line 2 in Line 3, in the above for loop, by straightforward computations, one can see that

$$\underline{\mathbf{W}}_i = \underline{\mathbf{X}}^T * \underline{\mathbf{X}} * \underline{\mathbf{\Omega}}_i - \underline{\mathbf{W}} * \underline{\mathbf{Z}}^{-1} * \underline{\mathbf{W}}^T * \underline{\mathbf{\Omega}}_i.$$

So, using these changes, we can modify Algorithm 9 to Algorithm 11. Following [39], One step of the orthonormalization has been skipped to reduce the computing time with a slight accuracy drop.

---

**Algorithm 9:** Randomized fixed-precision algorithm [38]
 

---

**Input :** A tensor  $\underline{\mathbf{X}} \in \mathbb{R}^{I_1 \times I_2 \times I_3}$ ; an error bound  $\epsilon$ ; a block size  $b$  and a power iteration  $q$ .

**Output:**  $\underline{\mathbf{Q}} = [\underline{\mathbf{Q}}^{(1)}, \underline{\mathbf{Q}}^{(2)}, \dots, \underline{\mathbf{Q}}^{(i)}]$ ,  $\underline{\mathbf{B}} = \begin{bmatrix} \underline{\mathbf{B}}^{(1)} \\ \underline{\mathbf{B}}^{(2)} \\ \vdots \\ \underline{\mathbf{B}}^{(i)} \end{bmatrix}$  such that

$$\|\underline{\mathbf{X}} - \underline{\mathbf{Q}} * \underline{\mathbf{B}}\|_F < \epsilon \text{ and corresponding optimal tubal rank } R$$

```

1  $\underline{\mathbf{Q}} = \emptyset$ ,  $\underline{\mathbf{B}} = \emptyset$ ;
2  $E = \|\underline{\mathbf{X}}\|_F^2$ ;
3 for  $i = 1, 2, \dots$  do
4    $\underline{\Omega}^{(i)} = \text{randn}(I_2, b, I_3)$ ;
5    $\underline{\mathbf{Q}}^{(i)} = \text{orth}(\underline{\mathbf{X}} * \underline{\Omega}^{(i)} - \underline{\mathbf{Q}} * (\underline{\mathbf{B}} * \underline{\Omega}^{(i)}))$ ;
6   for  $j = 1, 2, \dots, q$  do
7      $\underline{\mathbf{Q}}^{(i)} = \text{orth}(\underline{\mathbf{X}}^T * \underline{\mathbf{Q}}^{(i)} - \underline{\mathbf{B}}^T * \underline{\mathbf{Q}}^T * \underline{\mathbf{Q}}^{(i)})$ ;
8      $\underline{\mathbf{Q}}^{(i)} = \text{orth}(\underline{\mathbf{X}} * \underline{\mathbf{Q}}^{(i)} - \underline{\mathbf{Q}} * \underline{\mathbf{B}} * \underline{\mathbf{Q}}^{(i)})$ ;
9   end
10   $\underline{\mathbf{Q}}^{(i)} = \text{orth}(\underline{\mathbf{Q}}^{(i)} - \underline{\mathbf{Q}} * (\underline{\mathbf{Q}}^T * \underline{\mathbf{Q}}^{(i)}))$ ;
11   $\underline{\mathbf{B}}^{(i)} = \underline{\mathbf{Q}}^{(i)T} * \underline{\mathbf{X}}$ ;
12   $\underline{\mathbf{Q}} = \underline{\mathbf{Q}} \boxplus_2 \underline{\mathbf{Q}}^{(i)}$ ;
13   $\underline{\mathbf{B}} = \underline{\mathbf{B}} \boxplus_1 \underline{\mathbf{B}}^{(i)}$ ;
14   $E = E - \|\underline{\mathbf{B}}^{(i)}\|_F^2$ ;
15  if  $E < \epsilon^2$  then
16    | Break
17  end
18 end

```

---

---

**Algorithm 10:** Proposed fixed-precision algorithm I

---

**Input :** The data tensor  $\underline{\mathbf{X}} \in \mathbb{R}^{I_1 \times I_2 \times I_3}$  ( $I_1 \leq I_2$ ), an approximation error bound  $\epsilon$ , the pass numbers  $q > 2$  and block size  $b$

**Output:** A low tubal rank approximation of the tensor  $\underline{\mathbf{X}} \approx \underline{\mathbf{Q}} * \underline{\mathbf{R}}$ ;

```
1  $\underline{\mathbf{Q}} = []$ ;  $\underline{\mathbf{B}} = []$ ;  
2 for  $l = 1, 2, \dots$  do  
3   if if  $q$  is an even number then  
4      $\underline{\mathbf{\Omega}} = \text{randn}(I_2, b, I_3)$ ;  
5      $\underline{\mathbf{Y}} = \underline{\mathbf{X}} * \underline{\mathbf{\Omega}} - \underline{\mathbf{Q}} * (\underline{\mathbf{B}} * \underline{\mathbf{\Omega}})$ ;  
6      $[\underline{\mathbf{Q}}_l, \sim] = \text{T-LU}(\underline{\mathbf{Y}})$ ;  
7   else  
8     Set  $\underline{\mathbf{Q}}_l$  as a random tensor of size  $I_1 \times b \times I_3$ ;  
9   end  
10  for  $t = 1, 2, \dots, \lfloor \frac{q-2}{2} \rfloor$  do  
11    if  $t == \lfloor \frac{q-2}{2} \rfloor$  then  
12       $\underline{\mathbf{R}} = \underline{\mathbf{X}}^T * \underline{\mathbf{Q}}_l$ ;  
13       $\underline{\mathbf{Q}}_l = \text{orth}(\underline{\mathbf{X}} * \underline{\mathbf{R}} - \underline{\mathbf{Q}} * (\underline{\mathbf{B}} * \underline{\mathbf{R}}))$ ;  
14    else  
15       $[\underline{\mathbf{Q}}_l, \sim] = \text{T-LU}(\underline{\mathbf{X}} * (\underline{\mathbf{X}}^T * \underline{\mathbf{Q}}_l))$ ;  
16    end  
17  end  
18   $\underline{\mathbf{Q}}_l = \text{orth}(\underline{\mathbf{Q}}_l - \underline{\mathbf{Q}}_l * (\underline{\mathbf{Q}}^T * \underline{\mathbf{Q}}_l))$ ;  
19   $\underline{\mathbf{B}}_l = \underline{\mathbf{Q}}_l^T * \underline{\mathbf{X}}$ ;  
20   $\underline{\mathbf{Q}} = \underline{\mathbf{Q}} \boxplus_2 \underline{\mathbf{Q}}_l$ ;  
21   $\underline{\mathbf{B}} = \underline{\mathbf{B}} \boxplus_1 \underline{\mathbf{B}}_l$ ;  
22  if a termination criterion is satisfied then  
23    Set the tubal rank as  $k$  and break;  
24  end  
25 end
```

---

---

**Algorithm 11:** The proposed fixed-precision algorithm II
 

---

**Input :** The data tensor  $\underline{\mathbf{X}} \in \mathbb{R}^{I_1 \times I_2 \times I_3}$ , a block size  $b$ , a power iteration  $q$  and an approximation error bound.

**Output:** The QB approximation of the tensor  $\|\underline{\mathbf{X}} - \underline{\mathbf{Q}} * \underline{\mathbf{B}}\|_F \leq \epsilon$

```

1  $\underline{\mathbf{Y}} = \mathbf{[]}$ ,  $\underline{\mathbf{W}} = \mathbf{[]}$ ;
2  $E = \|\underline{\mathbf{X}}\|_F$ ,  $tol = \epsilon^2$ ;
3 for  $i = 1, 2, \dots$  do
4   Generate a random tensor  $\underline{\Omega}_i$  of size  $I_2 \times b \times I_3$ ;
5   for  $j = 1, 2, \dots, q$  do
6      $\underline{\mathbf{W}}_i = \underline{\mathbf{X}}^T * \underline{\mathbf{X}} * \underline{\Omega}_i - \underline{\mathbf{W}} * \underline{\mathbf{Z}}^{-1} * \underline{\mathbf{W}}^T * \underline{\Omega}_i$ ;
7      $\underline{\Omega}_i = \text{orth}(\underline{\mathbf{W}}_i)$ ;
8   end
9    $\underline{\mathbf{Y}}_i = \underline{\mathbf{X}} * \underline{\Omega}_i$ ,  $\underline{\mathbf{W}}_i = \underline{\mathbf{X}}^T * \underline{\mathbf{Y}}_i$ ;
10   $\underline{\mathbf{Y}} = \underline{\mathbf{Y}} \boxplus_2 \underline{\mathbf{Y}}_i$ ,  $\underline{\mathbf{W}} = \underline{\mathbf{W}} \boxplus_2 \underline{\mathbf{W}}_i$ ;
11   $\underline{\mathbf{Z}} = \underline{\mathbf{Y}}^T * \underline{\mathbf{Y}}$ ,  $\underline{\mathbf{T}} = \underline{\mathbf{W}}^T * \underline{\mathbf{W}}$ ;
12  if  $E - (\text{trace}((\underline{\mathbf{T}} * \underline{\mathbf{Z}}^{-1})_1)) < tol$  then
13    break
14  end
15 end
16  $[\widehat{\mathbf{V}}, \widehat{\mathbf{D}}] = \text{T-EIG}(\underline{\mathbf{Z}})$ ;
17  $\underline{\mathbf{Q}} = \underline{\mathbf{Y}} * \widehat{\mathbf{V}} * \text{sqrt}(\widehat{\mathbf{D}})^{-1}$ ,  $\underline{\mathbf{B}} = (\underline{\mathbf{W}} * \widehat{\mathbf{V}} * \text{sqrt}(\widehat{\mathbf{D}})^{-1})^T$ ;

```

---

## 6. Experimental results

In this section, we check the performance of Algorithms 6 and 7 on the synthetic and real-world data tensors. We conducted our experiments using MATLAB and on a computer with a 2.60 GHz Intel(R) Core(TM) i7-5600U processor and 8GB memory.

The first experiment is for the synthetic data. The second and third experiments are for image and video compression tasks. The last two experiments show applications of the proposed approaches to the image super-resolution and deep learning tasks.

The PSNR of two images  $\underline{\mathbf{X}}$  and  $\underline{\mathbf{Y}}$  is defined as

$$\text{PSNR} = 10 \log_{10} \left( \frac{255^2}{\text{MSE}} \right) \text{ dB},$$

where  $\text{MSE} = \frac{\|\underline{\mathbf{X}} - \underline{\mathbf{Y}}\|_F^2}{\text{num}(\underline{\mathbf{X}})}$  and "num( $\underline{\mathbf{X}}$ )" stands for the number of elements of the data tensor  $\underline{\mathbf{X}}$ . The relative error is also defined as

$$e(\underline{\tilde{\mathbf{X}}}) = \frac{\|\underline{\mathbf{X}} - \underline{\tilde{\mathbf{X}}}\|_F}{\|\underline{\mathbf{X}}\|_F},$$

where  $\underline{\mathbf{X}}$  is the original tensor and  $\underline{\tilde{\mathbf{X}}}$  is the approximated tensor.

**Example 1. (Synthetic data tensors)** In this example, we compare the efficiency of the proposed algorithms and baselines for the synthetic data tensors. Let us generate a random tensor with a low tubal rank approximation. To do so, we first consider a noiseless tensor  $\underline{\mathbf{X}} \in \mathbb{R}^{I_1 \times I_1 \times I_1}$  of the tubal rank  $R$  as follows

$$\underline{\mathbf{X}}_{clean} = \text{randn}(I_1, R, I_3) * \text{randn}(R, I_1, I_3), \quad (19)$$

and add a noise term to it to generate a noisy tensor  $\underline{\mathbf{X}}_{clean} + \delta \frac{\underline{\mathbf{Y}}}{\|\underline{\mathbf{Y}}\|_F} \|\underline{\mathbf{X}}_{clean}\|_F$  where  $\underline{\mathbf{Y}}$  is a standard Gaussian tensor of the same size as the original tensor  $\underline{\mathbf{X}}$ . We set  $r = 50$ ,  $\delta = 10^{-3}$  and assume  $I_1 = I_2 = I_3$  in all our simulations. So, the tubal rank of the tensor  $\underline{\mathbf{X}}_{clean}$  is approximately equal to 50, and we checked how accurate the proposed fixed-precision algorithms are to estimate this tubal rank. For a given error tolerance  $\epsilon = 10^{-5}$  and block size  $b = 100$ , the proposed fixed-precision algorithms 10-11 and the baselines methods including algorithm 9 and the truncated T-SVD are applied to the mentioned data tensor  $\underline{\mathbf{X}}_{clean}$ . Note that Algorithms 9-11 can estimate the tubal rank automatically, while the truncated

Table 1: The comparison of the proposed algorithm’s running times and relative errors and the truncated t-SVD, for example, 1. The entries represent (Computing time and relative error).

Tensor size	Algorithm 9	Algorithm 10	Algorithm 11	Truncated T-SVD
$n = 200$	(2.94, 2.95e-10)	(2.71, 2.58e-09)	(1.18, 4.72e-09)	(11.43, 1.34e-09)
$n = 300$	(8.74, 6.47e-10)	(4.21, 6.95e-09)	(3.07, 9.20e-09)	(36.81, 1.17e-09)
$n = 400$	(20.86, 1.15e-09)	(7.98, 1.27e-08)	(6.65, 1.63e-08)	(81.83, 2.11e-09)
$n = 500$	(45.89, 1.90e-09)	(20.59, 2.34e-08)	(19.32, 1.61e-08)	(195.25, 3.43e-09)

T-SVD requires the tubal rank as an input. Because of this issue, as mentioned, we first estimated the tubal rank using the fixed-precision algorithms 9-11, and then the estimated tubal rank was used in the truncated T-SVD. Our first observation was that all fixed-precision algorithms estimated the tubal rank correctly, but the CPU time of the proposed algorithms was relatively lower than the baseline Algorithm 9.

Also, for the tubal rank  $R = 50$ , we applied the truncated T-SVD for the tensor  $\underline{\mathbf{X}}_{clean}$ . Here, the running time of the truncated T-SVD was significant compared to the proposed fixed-precision algorithms, while its accuracy was almost the same as that of the proposed randomized algorithms. We also observe that as the tensor size increases, the proposed algorithms’ running times are much less than the baselines. These observations convinced us that the proposed fixed-precision algorithms are faster and more efficient than the baselines.

The simulation results, including the relative error and computing time of the proposed randomized fixed-precision algorithms and the baselines, including algorithm 9 and the truncated T-SVD for  $I_1 = 200, 300, 400$  and the tubal rank  $R = 50$ , are reported in Table 1. The results obviously show that the proposed randomized fixed-precision algorithms can provide more accurate approximations compared to the baselines in much less computing time.

Furthermore, to assess the performance of the proposed randomized single-pass algorithms 6-8, we applied them to the tensor (19) with  $I_1 = 300$  and  $R = 50$  and compared them with the baseline algorithms 4-5. For Algorithms 6-8, we used the sketch parameters  $L = K = 50, H = 45, R = 40$ , and for Algorithms 4-5, we used  $L = K = 40$ . So, all algorithms compute a low tubal rank approximation of tubal rank  $R = 40$ . These results are shown in Table 2. The running time of the proposed single-pass algorithms is a little higher than the baselines, as we see in Table 2, but they are more stable in selecting the sketch sizes. We will see in example 2 that the sensitivity of Algorithms 4-5 to the sketch parameters  $L = K$  is more serious, and the proposed algorithms are more reliable.

To further evaluate the performance of the proposed algorithms, let us now



Table 2: The comparison of computing times and relative errors of the proposed algorithms and the truncated t-SVD for the tensor (19) in Example 1 of size  $300 \times 300 \times 300$  and the tubal rank 40. The entries represent (Computing time and relative error).

Algorithm 4	Algorithm 5	Algorithm 6	Algorithm 7	Algorithm 8
(2.96, 5.75)	(4.97, 8.10)	(9.60, 0.26)	(9.01, 0.26)	(12.18, 0.26)

consider three new synthetic data tensors defined as follows:

- Tensor Case I:  $\underline{\mathbf{X}}(i, j, k) = \frac{1}{\sqrt{i^2+j^2+k^2}}$
- Tensor Case II:  $\underline{\mathbf{Y}}(i, j, k) = \frac{1}{(i^3+j^3+k^3)^{1/3}}$
- Tensor Case III:  $\underline{\mathbf{X}}(i, j, k) = \frac{1}{\sin(i)+\tanh(j+k)}$

We applied the proposed single-pass and baseline algorithms 5-6 to the mentioned tensors of size  $300 \times 300 \times 300$  with the tubal rank  $R = 40$ . The obtained numerical results reported in Table 3 demonstrate the robustness of the proposed algorithms compared to the baselines. These simulations convinced us that the proposed algorithm is more efficient than the other techniques.

Table 3: The comparison of computing times and relative errors of the proposed algorithms and the truncated t-SVD for tensors Cases I-III in Example 1. The entries represent (Computing time and relative error).

Data Tensor Case I				
Algorithm 4	Algorithm 5	Algorithm 6	Algorithm 7	Algorithm 8
(1.6, 0.07)	(3.6, 2.81e-14)	(7.7, 1.91e-14)	(7.6, 1.26e-14)	(6.3, 3.04e-14)
Data Tensor Case I				
Algorithm 4	Algorithm 5	Algorithm 6	Algorithm 7	Algorithm 8
(1.5, 0.014)	(3.10, 3.62e-12)	(7.00, 2.80e-14)	(7.45, 5.79e-14)	(9.32, 2.92e-14)
Data Tensor Case II				
Algorithm 4	Algorithm 5	Algorithm 6	Algorithm 7	Algorithm 8
(1.62, 2.60)	(3.53, 8.50e-15)	(7.35, 1.91e-14)	(7.54, 2.36e-14)	(6.23, 5.19e-14)

**Example 2. (Image Compression)** We examine the effectiveness of the suggested randomized single-pass algorithms for the image compression problem in this experiment. We used the Kodak dataset <sup>3</sup> and considered four images,

<sup>3</sup><https://r0k.us/graphics/kodak/>

"Kodim15", "Kodim17", "Kodim18," and "Kodim23" in our simulations. The first two images are of size  $512 \times 768 \times 3$  while the second two images are of size  $768 \times 512 \times 3$ . We applied our proposed algorithms and compared them with the baselines single-pass T-CUR [37] and tensor Sketch [32]. In our simulations we set sketches  $L = 350$ ,  $K = 350$ ,  $H = 100$  and  $R = 30$ . The reconstructed images with corresponding PSNR and relative errors are reported in Figure 3. The results demonstrate that our proposed randomized single-pass algorithms provided better results than the single-pass T-CUR and the tensor Sketch algorithms. It is interesting to report that we found experimentally that when we set  $K = L$ , all algorithms except the proposed randomized single-pass Algorithms 6-8 were unstable and provided poor results. In this sense, our algorithm 7 can be more reliable. Better results are achieved as soon as the sketch parameters are different  $L \neq K$ . The next numerical finding, which we should point out, is that for the case of  $L < K$ , the results were poor, and in all experiments, this was the case. This instability is due to the ill-conditioning of the underlying least-squares problem, which needs to be solved. More precisely, the Moore-Penrose of the coefficient tensor, according to the least-squares problem, is poorly computed, and the final results are not satisfactory. However, the proposed randomized single-pass Algorithms 6-8 are robust because truncated T-SVD in lines (6-7) act as regularizers and improve the numerical efficiency. This illustration amply demonstrates how the suggested approach is more reliable and capable of producing superior results.

**Example 3. (Video compression)** In this example, we study the performance of the proposed randomized single-pass algorithms for the video compression task. We mainly use the videos datasets "Foreman" and "News"<sup>4</sup>. The size of these videos are third-order tensors of size  $144 \times 176 \times 300$ . First, we tested the efficiency of the single-pass algorithms for low tubal rank approximations for the mentioned videos using the sketch parameters  $K = 90$ ,  $L = 90$ ,  $H = 20$ , and  $R = 20$ . The PSNR of all frames of the Foreman and News videos achieved by the proposed single-pass algorithms and the baselines are reported in Figures 4 and 5, respectively. Also, the reconstructed images of some frames of the mentioned videos are displayed in figures 6 and 7, respectively. We see that the proposed Algorithms 6-8 are robust in terms of the sketch sizes used, and this example illustrates the reliability of the proposed randomized single-pass algorithms for compressing videos.

---

<sup>4</sup><http://trace.eas.asu.edu/yuv/>



Figure 3: Reconstructed images using different single-pass algorithms for sketch sizes  $L = 350$ ,  $K = 350$ ,  $H = 100$  and  $R = 30$ . The results show a better performance of the proposed randomized single-pass algorithms.

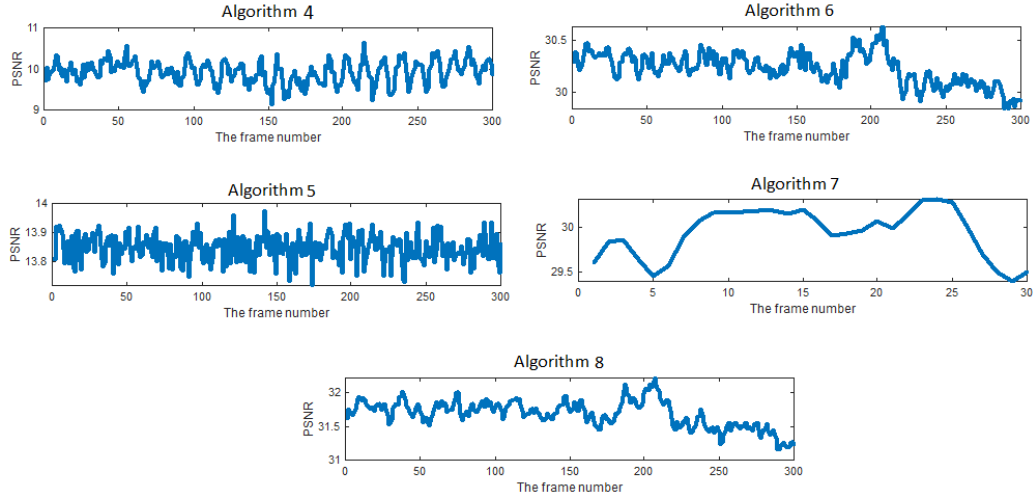


Figure 4: The PSNR of all frames of the Foreman video was achieved using different single-pass algorithms for sketch sizes  $L = 90, K = 90, H = 20$  and  $R = 50$ . The results show a better performance of the proposed randomized single-pass algorithms.

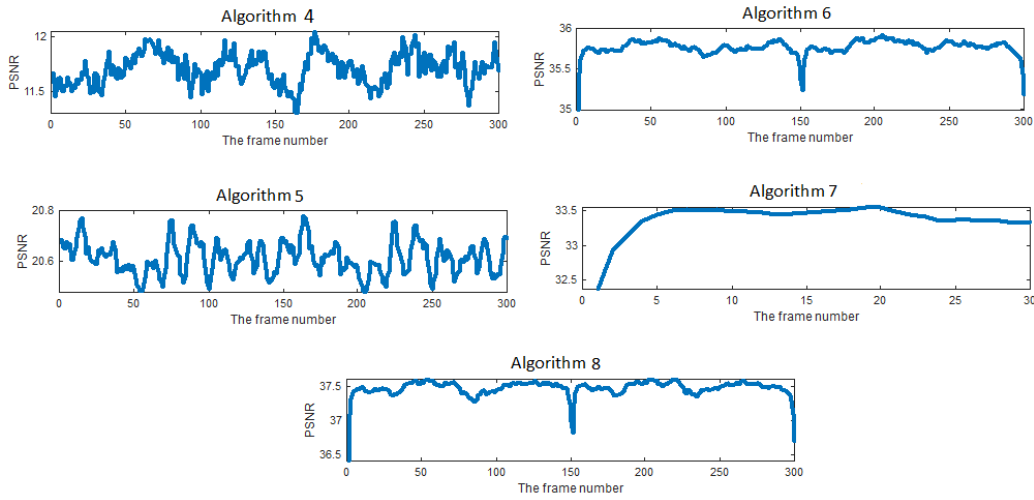


Figure 5: The PSNR of all frames of the News Video was achieved using different single-pass algorithms for sketch sizes  $L = 90, K = 90, H = 20$  and  $R = 50$ . The results show a better performance of the proposed randomized single-pass algorithms.



Figure 6: The reconstruction of some random frames of the Foreman Video obtained using different single-pass algorithms for sketch sizes  $L = 90$ ,  $K = 90$ ,  $H = 20$  and  $R = 50$ . The results show a better performance of the proposed randomized single-pass algorithms.



Figure 7: The reconstruction of some random frames of the News Video obtained using different single-pass algorithms for sketch sizes  $L = 90$ ,  $K = 90$ ,  $H = 20$  and  $R = 50$ . The results show a better performance of the proposed randomized single-pass algorithms.

**Example 4. (Image Super-resolution)** . In this experiment, we study the efficiency and applicability of the proposed approaches to the super-resolution task. The super-resolution is an important computer vision task that involves reconstructing a higher-resolution image from an input image with a lower resolution. The goal is to provide a more aesthetically pleasant and detailed image while reducing artifacts and noise. The image super-resolution can be solved via tensor completion. More precisely, a given small image is up-sampled in the first and second dimensions, and an incomplete image is obtained. Then, the tensor completion can be applied to this incomplete image to recover the missing pixels. We adopt the tensor completion proposed in [13] for this task. To the best of our knowledge, this is the first paper using single-pass algorithms for tensor completion and image super-resolution. Here, the following iterative steps<sup>5</sup>

$$\underline{\mathbf{X}}^{(n)} \leftarrow \mathcal{L}(\underline{\mathbf{C}}^{(n)}), \quad (20)$$

$$\underline{\mathbf{C}}^{(n+1)} \leftarrow \underline{\mathbf{C}}^{(0)} + (\underline{\mathbf{1}} - \underline{\mathbf{\Omega}}) \circledast \underline{\mathbf{X}}^{(n)}, \quad (21)$$

$n = 0, 1, 2, \dots$  are performed, where  $\underline{\mathbf{C}}^{(0)}$  is the initial image with missing elements  $\underline{\mathbf{M}}$ , and  $\mathcal{L}$  is an operator to compute a low tensor approximation of the tensor  $\underline{\mathbf{C}}^{(0)}$ . Here,  $\circledast$  stands for the Hadamard or element-wise multiplication of two tensors,  $\underline{\mathbf{1}}$  is a tensor of the same size as the original image all whose elements are equal to one, and the so-called mask tensor  $\underline{\mathbf{\Omega}}$  is a binary tensor specifying the location of known elements, that it if an element in the tensor is known the corresponding element in the binary tensor is 1 otherwise it is 0. The stages (20)-(21) are repeated until a given approximation error abound is satisfied or a maximum number of iterations (80 iterations) is reached. The first stage is expensive, and we use our proposed approach to find a low-rank tensor approximation. More precisely, we employed the proposed randomized single-pass algorithms. To further improve the image recovery after the second stage (21), we apply the Gaussian filter (the MATLAB function “imgaussfilt”). Fives images ”Peppers“, ”Airplane“, ”Kodim01“, ”Kodim02“ and ”Kodim03“ are considered. The first two images are of size  $256 \times 256 \times 3$  while the next three images are of size  $512 \times 768 \times 3$ . The images are upsampled 4 times along the x-axis and y-axis, and the tubal rank  $R = 60$  is used for all images.

The simulation results are reported in Table 4, and two reconstructed images are shown in Figure 8. From the results of Table 4, we see that the proposed

---

<sup>5</sup>We skip the derivation details due to space limitation. The readers are referred to [13] for more details.

Table 4: The comparison of running times and relative errors of the proposed algorithm and the truncated T-SVD, for Example, 4. The entries represent (Computing time and PSNR).

Image	Single-pass completion	Deterministic completion
Peppers	(26.99, 22.01)	(42.70, 22.01)
Airplane	(27.69, 22.13)	(44.58, 22.11)
Kodim01	(50.34, 20.44)	(142.42, 20.56)
Kodim02	(44.58, 26.70)	(137.30, 26.91)
Kodim03	(48.05, 26.96)	(146.76, 27.42)



Figure 8: The super-resolution results obtained via the tensor completion algorithm using the proposed randomized single-pass algorithms for low tubal computation for the operator  $\mathcal{L}$  in (20).

randomized fixed-precision algorithms provide similar recovered images in much less computing time compared to the deterministic one (truncated T-SVD). This shows the advantage of the proposed randomized single-pass algorithms in the image super-resolution task.

**Example 5. (Deep Learning Application)** In this example, we consider the application of the proposed completion method in accurate object detection as an important computer vision task in deep learning. To be more precise, we consider two images shown (we call them “dog” and “horses”) in Figure 9 (first row) and manually remove some parts of the images structurally depicted in Figure 9 (second row).

We consider the retrained YOLO3 (You Only Look Once, Version 3) an efficient deep neural network for object detection [44]. YOLOv3 is an improvement over its predecessor, YOLOv2 [45], and aims to address some of the limitations of earlier versions. It is known for its speed and efficiency in real-time object detection tasks. YOLOv3 divides the input image into a grid and predicts bounding boxes and class probabilities for each grid cell. This allows for faster processing compared to other object detection algorithms that scan the entire image multiple



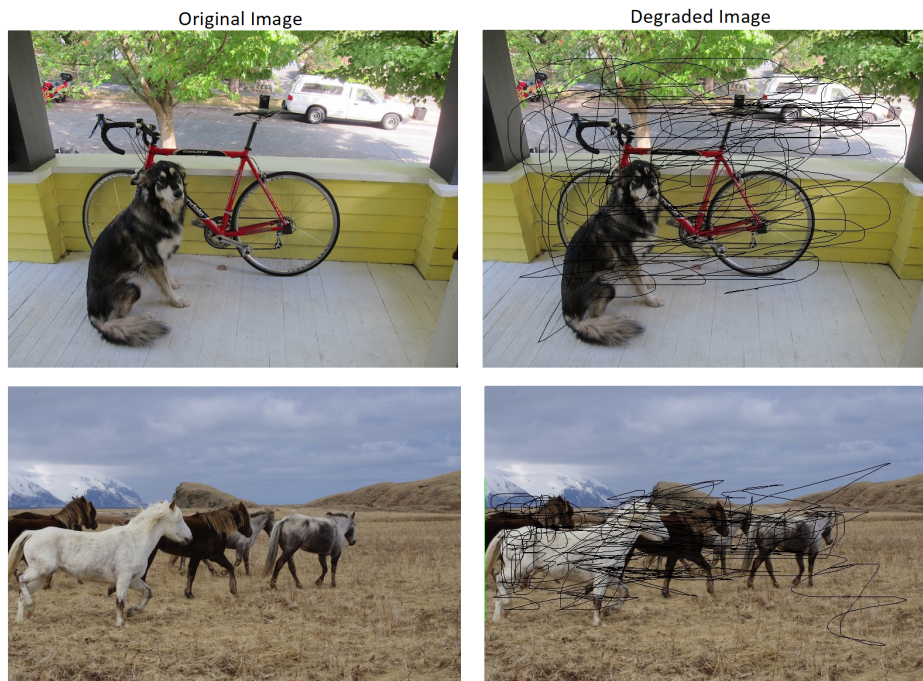


Figure 9: The original and degraded images used in our experiments.

times. It is known that YOLOv3 has become a popular choice for real-time object detection tasks due to its speed, accuracy, and efficiency.

We considered the YOLO3 and applied this network to detect objects in degraded images. These results are shown in Figure 9 (first row). As can be seen, the network for the dog image only detected one object (cat), which is also not correct. The network also detects two objects for the horse image: one horse and one giraffe. It failed to detect two additional horses and also incorrectly detected a horse as a giraffe. In contrast, as a preprocessing stage, our completion technique first quickly processes the degraded image, and then the YOLO3 is applied to it to detect the objects inside the image. After the fast preprocessing using our techniques, the network detected three objects for the dog image: a bicycle, a dog, and a truck with very precise bounding boxes. Also, for the horse's image, the network detected four horses. The results clearly show the efficiency and feasibility of the proposed completion procedure for stabilizing YOLO3 against pixel removal.

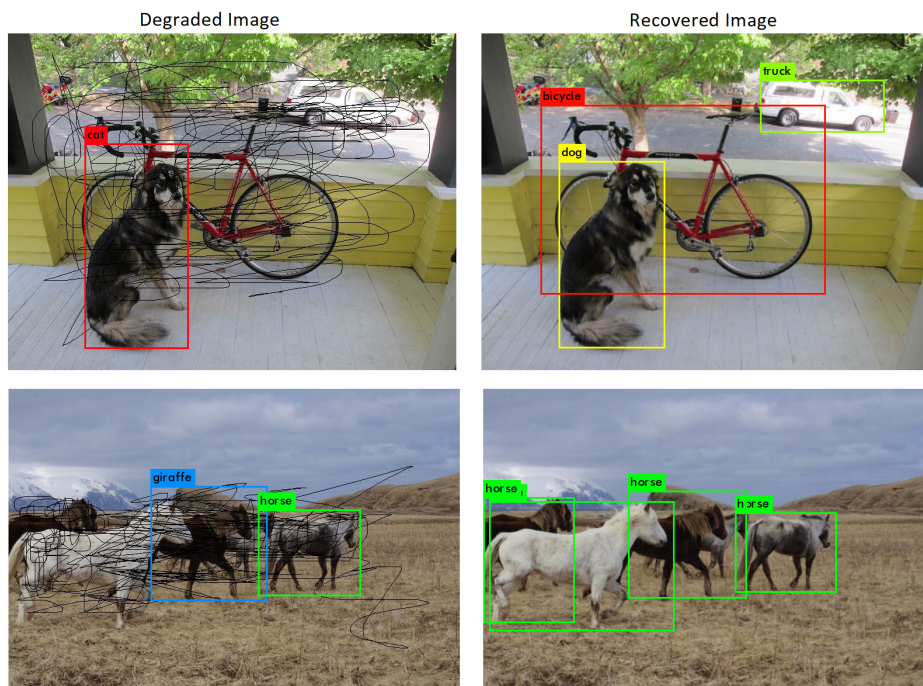


Figure 10: The object detection results obtained from the degraded images and those after recovering via the tensor completion algorithm with the proposed randomized single-pass algorithms.

## 7. Conclusion

This paper proposed efficient single-pass and fixed-precision algorithms to compute low tubal rank approximations of third-order tensors. We first developed three new single-pass algorithms for low tubal rank approximation and studied their robustness for approximating images and videos. Our simulation results confirmed that the proposed single-pass algorithms are more robust than the existing baselines. Applications of the proposed single-pass algorithms in data compression, image super-resolution, and deep learning were also presented. In the second part of the paper, we proposed two new fixed-precision algorithms for the low tubal rank approximation. The experiments were also conducted to evaluate the proposed fixed-precision algorithms. The results show that the proposed algorithms provide better results than the state-of-the-art ones in less computing times.

## 8. Conflict of Interest Statement

The authors declare that they have no conflict of interest with anything.

## References

- [1] L. R. Tucker, et al., The extension of factor analysis to three-dimensional matrices, *Contributions to mathematical psychology* 110119 (1964).
- [2] L. De Lathauwer, B. De Moor, J. Vandewalle, A multilinear singular value decomposition, *SIAM journal on Matrix Analysis and Applications* 21 (4) (2000) 1253–1278.
- [3] I. V. Oseledets, Tensor-train decomposition, *SIAM Journal on Scientific Computing* 33 (5) (2011) 2295–2317.
- [4] Q. Zhao, G. Zhou, S. Xie, L. Zhang, A. Cichocki, Tensor ring decomposition, *arXiv preprint arXiv:1606.05535* (2016).
- [5] Y. Znyed, R. Boyer, A. L. F. de Almeida, G. Favier, A TT-based hierarchical framework for decomposing high-order tensors, *SIAM Journal on Scientific Computing* 42 (2) (2020) A822–A848.

- [6] M. E. Kilmer, K. Braman, N. Hao, R. C. Hoover, Third-order tensors as operators on matrices: A theoretical and computational framework with applications in imaging, *SIAM Journal on Matrix Analysis and Applications* 34 (1) (2013) 148–172.
- [7] A. H. Phan, A. Cichocki, P. Tichavský, D. P. Mandic, K. Matsuoka, On revealing replicating structures in multiway data: A novel tensor decomposition approach, in: *Latent Variable Analysis and Signal Separation: 10th International Conference, LVA/ICA 2012, Tel Aviv, Israel, March 12-15, 2012. Proceedings 10*, Springer, 2012, pp. 297–305.
- [8] A. H. Phan, A. Cichocki, P. Tichavský, R. Zdunek, S. Lehky, From basis components to complex structural patterns, in: *2013 IEEE International Conference on Acoustics, Speech and Signal Processing, IEEE, 2013*, pp. 3228–3232.
- [9] A.-H. Phan, A. Cichocki, P. Tichavský, G. Luta, A. Brockmeier, Tensor completion through multiple kronecker product decomposition, in: *2013 IEEE International Conference on Acoustics, Speech and Signal Processing, IEEE, 2013*, pp. 3233–3237.
- [10] A. L. F. de Almeida, G. Favier, J. C. M. Mota, A constrained factor decomposition with application to MIMO antenna systems, *IEEE Transactions on Signal Processing* 56 (6) (2008) 2429–2442.
- [11] A. Stegeman, A. L. F. de Almeida, Uniqueness conditions for constrained three-way factor decompositions with linearly dependent loadings, *SIAM J. Mat. Anal. Appl.* 31 (3) (2010) 1469–1490.
- [12] M. G. Asante-Mensah, S. Ahmadi-Asl, A. Cichocki, Matrix and tensor completion using tensor ring decomposition with sparse representation, *Machine Learning: Science and Technology* 2 (3) (2021) 035008.
- [13] S. Ahmadi-Asl, M. G. Asante-Mensah, A. Cichocki, A. H. Phan, I. Oseledets, J. Wang, Fast cross tensor approximation for image and video completion, *Signal Processing* (2023) 109121.
- [14] E. Frolov, I. Oseledets, *Tensor methods and recommender systems*, Wiley Interdisciplinary Reviews: Data Mining and Knowledge Discovery 7 (3) (2017) e1201.

- [15] N. D. Sidiropoulos, L. De Lathauwer, X. Fu, K. Huang, E. E. Papalexakis, C. Faloutsos, Tensor decomposition for signal processing and machine learning, *IEEE Transactions on signal processing* 65 (13) (2017) 3551–3582.
- [16] L. Eldén, S. Ahmadi-Asl, Solving bilinear tensor least squares problems and application to hammerstein identification, *Numerical Linear Algebra with Applications* 26 (2) (2019) e2226.
- [17] A. L. de Almeida, G. Favier, J. C. M. Mota, Parafac-based unified tensor modeling for wireless communication systems with application to blind multiuser equalization, *Signal Processing* 87 (2) (2007) 337–351, *tensor Signal Processing*.
- [18] A. L. F. de Almeida, G. Favier, J. P. C. L. da Costa, J. C. M. Mota, Overview of tensor decompositions with applications to communications, in: R. Coelho, V. Nascimento, R. de Queiroz, J. Romano, C. Cavalcante (Eds.), *Signals and Images: Advances and Results in Speech, Estimation, Compression, Recognition, Filtering, and Processing*, no. Chapter 12, CRC-Press, 2016, pp. 325–356.
- [19] G. Favier, A. L. F. de Almeida, Overview of constrained PARAFAC models, *EURASIP Journal on Advances in Signal Processing* 2014 (142) (9 2014).
- [20] A. L. F. de Almeida, G. Favier, J. C. M. Mota, A constrained factor decomposition with application to mimo antenna systems, *IEEE Transactions on Signal Processing* 56 (6) (2008) 2429–2442. doi:10.1109/TSP.2008.917026.
- [21] G. Favier, A. L. F. de Almeida, Tensor space-time-frequency coding with semi-blind receivers for MIMO wireless communication systems, *IEEE Trans. Signal Process.* 62 (22) (2014) 5987–6002. doi:10.1109/TSP.2014.2357781.
- [22] S. Ahmadi-Asl, A. Cichocki, A. H. Phan, M. G. Asante-Mensah, M. M. Ghazani, T. Tanaka, I. Oseledets, Randomized algorithms for fast computation of low rank tensor ring model, *Machine Learning: Science and Technology* 2 (1) (2020) 011001.
- [23] S. Ahmadi-Asl, S. Abukhovich, M. G. Asante-Mensah, A. Cichocki, A. H. Phan, T. Tanaka, I. Oseledets, Randomized algorithms for computation of

- Tucker decomposition and higher order SVD (HOSVD), *IEEE Access* 9 (2021) 28684–28706.
- [24] M. Che, Y. Wei, Randomized algorithms for the approximations of Tucker and the tensor train decompositions, *Advances in Computational Mathematics* 45 (1) (2019) 395–428.
- [25] J. Zhang, A. K. Saibaba, M. E. Kilmer, S. Aeron, A randomized tensor singular value decomposition based on the t-product, *Numerical Linear Algebra with Applications* 25 (5) (2018) e2179.
- [26] Q. Song, H. Ge, J. Caverlee, X. Hu, Tensor completion algorithms in big data analytics, *ACM Transactions on Knowledge Discovery from Data (TKDD)* 13 (1) (2019) 1–48.
- [27] J. Warren, N. Marz, *Big Data: Principles and best practices of scalable real-time data systems*, Simon and Schuster, 2015.
- [28] Z. Zhang, S. Aeron, Exact tensor completion using t-svd, *IEEE Transactions on Signal Processing* 65 (6) (2016) 1511–1526.
- [29] N. Hao, M. E. Kilmer, K. Braman, R. C. Hoover, Facial recognition using tensor-tensor decompositions, *SIAM Journal on Imaging Sciences* 6 (1) (2013) 437–463.
- [30] C. Zeng, M. K. Ng, Decompositions of third-order tensors: Hosvd, t-svd, and beyond, *Numerical Linear Algebra with Applications* 27 (3) (2020) e2290.
- [31] M. E. Kilmer, C. D. Martin, Factorization strategies for third-order tensors, *Linear Algebra and its Applications* 435 (3) (2011) 641–658.
- [32] L. Qi, G. Yu, T-singular values and t-sketching for third order tensors, arXiv preprint arXiv:2103.00976 (2021).
- [33] S. Ahmadi-Asl, A.-H. Phan, A. Cichocki, A randomized algorithm for tensor singular value decomposition using an arbitrary number of passes, *Journal of Scientific Computing* 98 (1) (2024) 23.
- [34] C. Lu, J. Feng, Y. Chen, W. Liu, Z. Lin, S. Yan, Tensor robust principal component analysis with a new tensor nuclear norm, *IEEE transactions on pattern analysis and machine intelligence* 42 (4) (2019) 925–938.

- [35] J. A. Tropp, A. Yurtsever, M. Udell, V. Cevher, Practical sketching algorithms for low-rank matrix approximation, *SIAM Journal on Matrix Analysis and Applications* 38 (4) (2017) 1454–1485.
- [36] E. K. Bjarkason, Pass-efficient randomized algorithms for low-rank matrix approximation using any number of views, *SIAM Journal on Scientific Computing* 41 (4) (2019) A2355–A2383.
- [37] D. A. Tarzanagh, G. Michailidis, Fast randomized algorithms for t-product based tensor operations and decompositions with applications to imaging data, *SIAM Journal on Imaging Sciences* 11 (4) (2018) 2629–2664.
- [38] S. Ahmadi-Asl, An efficient randomized fixed-precision algorithm for tensor singular value decomposition, *Communications on Applied Mathematics and Computation* 5 (4) (2023) 1564–1583.
- [39] X. Feng, W. Yu, A fast adaptive randomized pca algorithm, in: *Proceedings of the Thirty-Second International Joint Conference on Artificial Intelligence, 2023*, pp. 3695–3704.
- [40] S. Ahmadi-Asl, C. F. Caiafa, A. Cichocki, A. H. Phan, T. Tanaka, I. Oslelede, J. Wang, Cross tensor approximation methods for compression and dimensionality reduction, *IEEE Access* 9 (2021) 150809–150838.
- [41] M. F. Kaloorazi, R. C. de Lamare, Subspace-orbit randomized decomposition for low-rank matrix approximations, *IEEE Transactions on Signal Processing* 66 (16) (2018) 4409–4424.
- [42] W. Yu, Y. Gu, Y. Li, Efficient randomized algorithms for the fixed-precision low-rank matrix approximation, *SIAM Journal on Matrix Analysis and Applications* 39 (3) (2018) 1339–1359.
- [43] X. Ding, W. Yu, Y. Xie, S. Liu, Efficient model-based collaborative filtering with fast adaptive pca, in: *2020 IEEE 32nd International Conference on Tools with Artificial Intelligence (ICTAI), IEEE, 2020*, pp. 955–960.
- [44] J. Redmon, A. Farhadi, Yolov3: An incremental improvement, *arXiv preprint arXiv:1804.02767* (2018).
- [45] J. Redmon, A. Farhadi, Yolo9000: better, faster, stronger, in: *Proceedings of the IEEE conference on computer vision and pattern recognition, 2017*, pp. 7263–7271.